Analysis of Variability in Estimates of Cell Proliferation Parameters for Cyton-Based Models Using CFSE-Based Flow Cytometry Data

H.T. Banks, D.F. Kapraun, Kathryn G. Link, and W. Clayton Thompson
Center for Research in Scientific Computation
North Carolina State University, Raleigh, NC 27695-8212

Cristina Peligero, Jordi Argilaguet, and Andreas Meyerhans
ICREA Infection Biology Lab, Department of Experimental and Health Sciences
Universitat Pompeu Fabra, 08003 Barcelona, Spain

November 4, 2013

Abstract

In this article we assess variability in cell proliferation dynamics observed for CD4+ and CD8+ T cells collected from two healthy donors. We review a recently developed class of models that incorporates the so-called "cyton model" for cell numbers into a conservation-based PDE model for cell population dynamics and describe a statistical model that relates CFSE-based flow cytometry data to such models. A parameter estimation scheme is summarized and then applied to a large body of data to assess experimental variability (variation in parameter estimates as identical experiments are replicated) and biological variability (differences in parameter estimates obtained for different donors and cell types) in the context of these models. Variability in the data obtained from replicated experiments is also discussed. The results of this study indicate that many of the cyton model parameters for describing cell proliferation can be reliably estimated using our approach; however, they also show that substantial changes to our mathematical model and/or experimental procedures may be required to ensure identifiability of the remaining cell proliferation parameters.

1 Introduction

The adaptive immune response is a major component of the human immune system's defense against invading pathogens. The adaptive immune system consists of B and T lymphocytes, which recognize invaders by specific cell surface receptors and exert their responses by soluble and cellular effector mechanisms. As the success of this system depends on the lymphocytes' capacity to proliferate in response to an infection, the ability to accurately predict this behavior in the presence of specific environmental stimuli has important implications for human health research in areas such as the treatment and prevention of infectious disease and immunosuppression for organ and tissue transplants. Such predictions can be made through the use of mathematical models.

Over the last half-century, many mathematical models have been proposed that attempt to describe the dynamics of a proliferating population of cells, but until fairly recently it has been a challenge to validate such models. The discovery of the intracellular dye carboxyfluorescein succinimidyl ester (CFSE) was a major milestone in overcoming this obstacle. CFSE was originally developed as a tool for labeling lymphocytes so that their movements within animal subjects could be tracked over many months [22], but subsequently researchers determined that the dye could also be used to monitor lymphocyte proliferation [16]. Also, through the use of fluorescently labeled antibodies specific to various lymphocyte surface markers, it is now possible to follow the proliferative behavior of specific types of lymphocytes [15].

In this study, we consider a mathematical model that incorporates the "cyton model" for cell numbers into a partial differential equation model for cell proliferation dynamics that is based upon the conservation of CFSE mass within a population of proliferating cells. Utilizing a weighted least squares parameter estimation scheme, we fit this model to CFSE-based flow cytometry data obtained for CD4+ and CD8+ T cells collected from two healthy donors. Measurements were made in triplicate on each of five days, making it possible to construct a considerable number of five-day data sets for each donor and cell type. In theory, each such data set should be very similar, so one might expect that a set of parameters for describing cell proliferation dynamics observed in one of the data sets should be essentially equivalent to those describing observations made using another of the data sets. By applying our parameter estimation scheme to each five-day data set, we are able to assess experimental variability in the estimates of the parameters characterizing a specific cyton-based mathematical model. Also, by collecting data from two different human donors and considering two specific cell types, we are able to make some observations concerning biological variablility in the cell proliferation parameters.

2 Data Collection Procedure

As discussed above, the goal of this study is to assess the experimental and biological variability in parameter estimates produced using CFSE-based flow cytometry data and cyton-based mathematical models. To obtain such data, we collected blood samples from two human donors and isolated peripheral blood mononuclear cells (PBMCs) from these samples. The PBMCs (hereafter referred to as just "cells") were then passed through a strainer to remove clumps of cells and stained with CFSE according to the standard protocol [15]. Forty-five minutes after CFSE staining, the cells were stimulated to divide by exposing them to phytohaemagglutinin (PHA), a nonspecific T cell mitogen. Then, approximately 1 million cells were placed into each of several "wells", which are typical containers for cell culture experiments. Each well contained approximately 1 mL of RPMI-1640/10% fetal calf serum (FCS), which is a typical nutrient medium for such experiments. For each one of the donors, three wells were "seeded" in this way for each of five measurement times in order to allow for measurements to be obtained in triplicate at each time point; thus, 15 wells were seeded per donor. Since two donors were considered, a total of 30 wells were seeded at the beginning of the experiment.

Here we note that, as cells proliferate, CFSE in a dividing mother cell is distributed to two daughter cells. The CFSE bound to the proteins inside cells also naturally degrades over time. Thus, there are two mechanisms by which the mass of CFSE per cell can decline: cell division and CFSE decay. Such a decline in CFSE per cell can be quantified by collecting cells from the wells at various points in time and passing them through a flow cytometer. So, at each of five time points corresponding to approximately 1, 2, 3, 4, and 5 days after PHA stimulation, we transferred the contents of one of the wells to a sample tube that contained a known number of "beads". (The number of beads in each sample tube is fixed and is reported by the manufacturer of the tubes.) The actual times for data collection coincided with 23.5, 46.0, 67.5, 94.5, and 117.5 hours after stimulation with PHA. In order to minimize disruption of proliferating cell populations, the contents of any given well were harvested only once; however, we remark that beginning on Day 3 (after the Day 3 measurement was made) one third of the nutrient medium in each *unused* well was exchanged with fresh medium every 24 hours and that this exchange of medium could have affected the cell cultures in the wells that were harvested after Day 3. The cells were then stained with fluorochrome-labeled antibodies (anti-CD3, anti-CD4, and anti-CD8) as well as the viability dye known as ViViD, which allows for the identification of dead cells that haven't yet disintegrated. A sample consisting of a fraction (about 10 to 50%) of the contents of the sample tube was then passed through a flow cytometer. During this process, the flow cytometer measured the fluorescence intensity (FI) at various wavelengths of each cell in the sample and counted the number of beads in the sample. Because we processed only a fraction of the contents of each tube, the "actual" cell counts for any given range of FI were obtained by scaling the observed counts upward by the ratio of known number of beads in the tube to counted beads for the sample. As mentioned above, this process was repeated using cells from three different wells (per donor) at each measurement time.

Because the FI emitted at wavelengths in the range 515 to 545 nm varies directly with the mass of CFSE within a cell [15, 22], this FI is a useful surrogate for CFSE mass. Also, because CFSE is allocated evenly (by assumption) to two daughter cells upon cell division, FI histograms associated with a population of

cells acquire more "peaks" as the cells divide asynchronously. In Figures 1 through 8, we present summary histograms for the data collected in our study. Each of these figures illustrates the preceding point.

As described in the preceding paragraph, the FI emitted in the "CFSE range" by a given cell may be taken to be synonymous with the mass of CFSE contained in that cell. Therefore, CFSE data can be used to validate a mathematical model describing cell population dynamics that is based upon mass conservation principles. Such a model is described in detail in Section 3. Furthermore, when cells have been labeled with other markers (as is the case for the experiments in this study), information about FI at other wavelengths can be used to distinguish between different types of cells (e.g., CD4+ versus CD8+ T cells, or living versus dead cells) [15].

In order to ascertain variability in parameters and measured data, we require a considerable number of data sets. To this end, we use various combinations of the triplicate samples collected on Days 1 through 5 to form a large number of time series data sets. Since three samples were collected on each of five days, there should be $3^5 = 243$ possible ways to form a five-day "longitudinal" data set for each donor. However, data for one of the samples corresponding to Donor 1 and Day 4 was not available due to an instrument problem; therefore, there are in fact only $3^4 \times 2 = 162$ possible ways to form a five-day data set for Donor 1. It should explicitly noted that data sets formed in this way *do not represent truly longitudinal data* because measurements corresponding to each time point were made using distinct cell cultures (wells). In this type of *in vitro* experiment (see, for example, [15], [13], [17], and [2]) *it is tacitly assumed that the populations of cells in each well are identical* (up until the moment cells are harvested from a particular well) in that they include the same numbers of total cells in the same proportions (according to cell type). This assumption allows one to interpret time series data sets formed as described above as having come from longitudinal observations. In reality, however, there can be considerable variation in the cell cultures in the various wells due to experimental error in the initial seeding of the wells. This issue will be discussed further in Section 5.

3 Mathematical Model

Here, we summarize a class of models originally proposed in [20] and further developed in [6] and [2]. We then identify the specific model to be considered for the purposes of our variability study.

3.1 Basic Label-Structured Model for Cell Densities

Let $n_i(t,x)$ be a structured density (in cells per unit FI), where i is a whole number representing a specific "generation" of cells (or number of divisions completed), t denotes the time elapsed (in hr) since some arbitrary starting time, and x denotes FI *induced by CFSE*. Also, let $\{\alpha_i(t)\}$, $\{\beta_i(t)\}$, and $v(t)$ denote exponential division rates, exponential death rates, and the CFSE exponential decay rate, respectively (all in hr^{-1}). Then the dynamics of a population of cells are described by

$$\begin{aligned} \frac{\partial n_0(t,x)}{\partial t} - v(t)\frac{\partial [x n_0(t,x)]}{\partial x} &= -(\alpha_0(t)+\beta_0(t))n_0(t,x) && \text{for } i=0, \\ \frac{\partial n_i(t,x)}{\partial t} - v(t)\frac{\partial [x n_i(t,x)]}{\partial x} &= -(\alpha_i(t)+\beta_i(t))n_i(t,x) + R_i(t,x) && \text{for } i \geq 1, \end{aligned} \tag{3.1}$$

where $x \geq 0$ and the "recruitment" terms are given by

$$R_i(t,x) = 4\alpha_{i-1}(t)n_{i-1}(t,2x) \tag{3.2}$$

for $i \geq 1$. The initial conditions are given by

$$n_i(t_0,x) = \begin{cases} \Phi(x) & \text{for } i=0, \\ 0 & \text{for } i \geq 1, \end{cases} \tag{3.3}$$

where t_0 indicates the time of the first observation and $\Phi(x)$ is the structured density for cells in the initial (undivided) population. A derivation of this model based on mass conservation principles can be found in

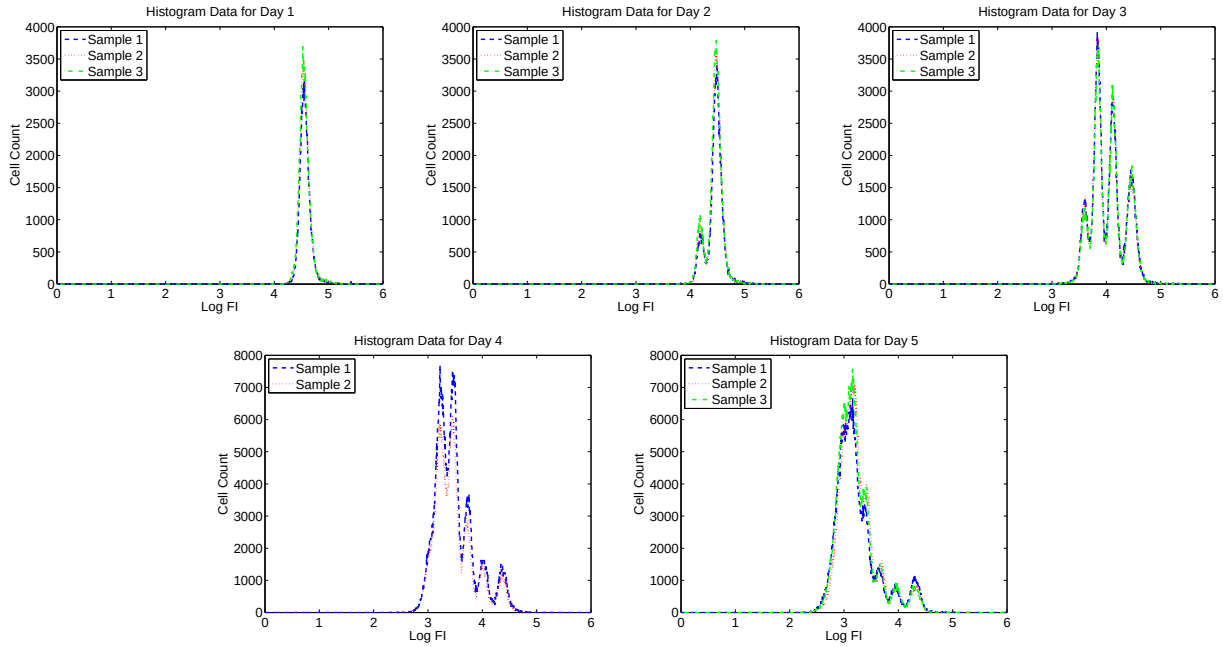

Figure 1: Summary histogram data for CD4+ T cells measured for Donor 1 using ViViD dye to exclude dead cells.

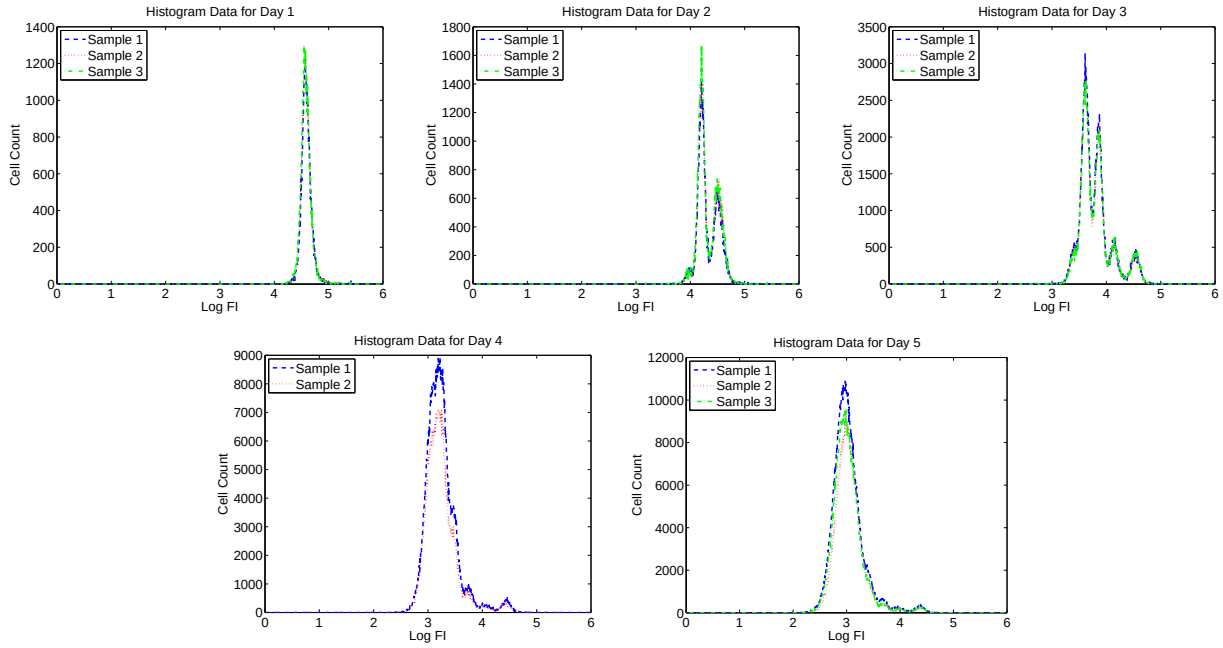

Figure 2: Summary histogram data for CD8+ T cells measured for Donor 1 using ViViD dye to exclude dead cells.

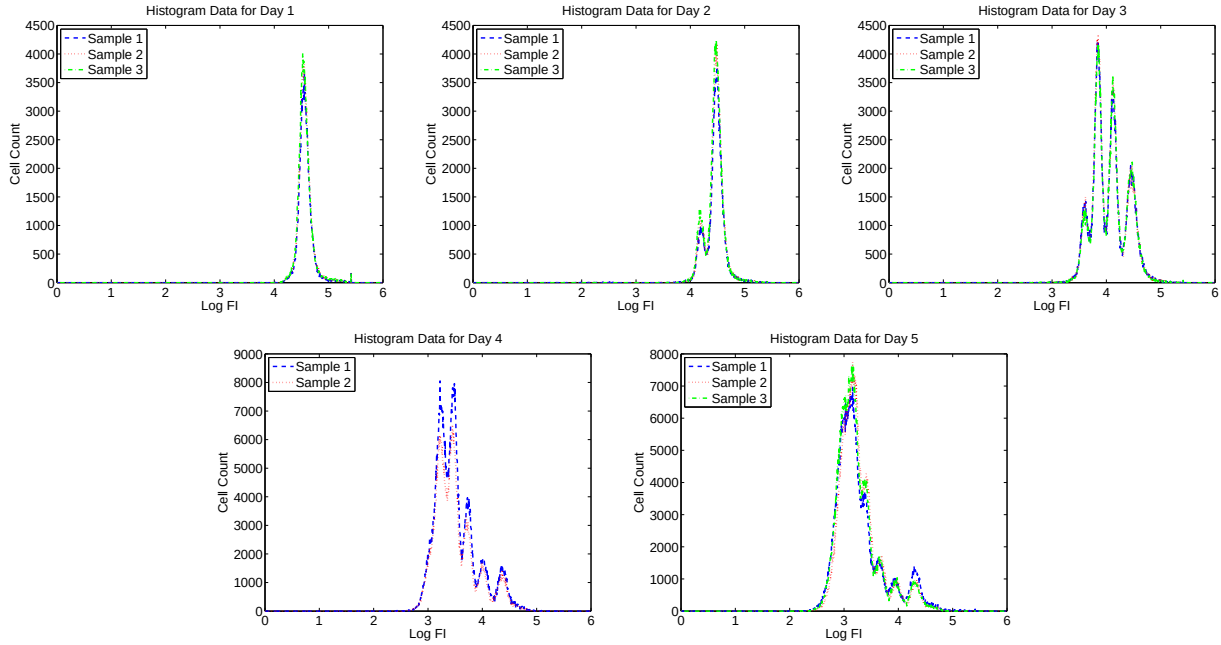

Figure 3: Summary histogram data for CD4+ T cells measured for Donor 1 without using ViViD dye to exclude dead cells.

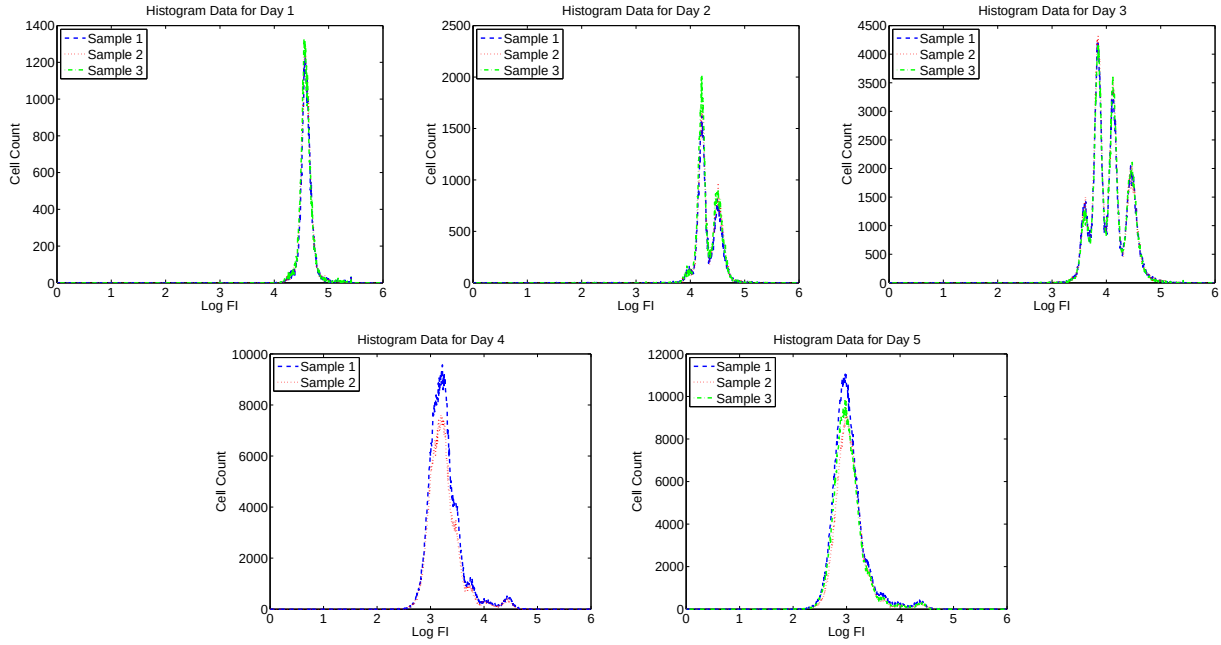

Figure 4: Summary histogram data for CD8+ T cells measured for Donor 1 without using ViViD dye to exclude dead cells.

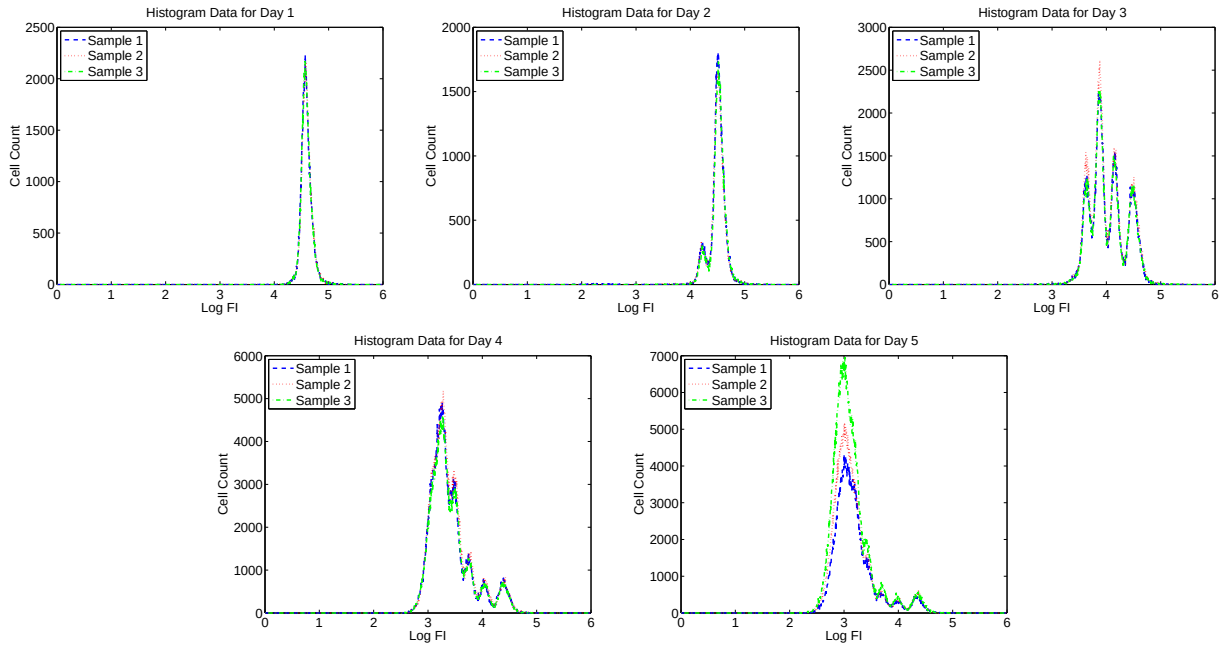

Figure 5: Summary histogram data for CD4+ T cells measured for Donor 2 using ViViD dye to exclude dead cells.

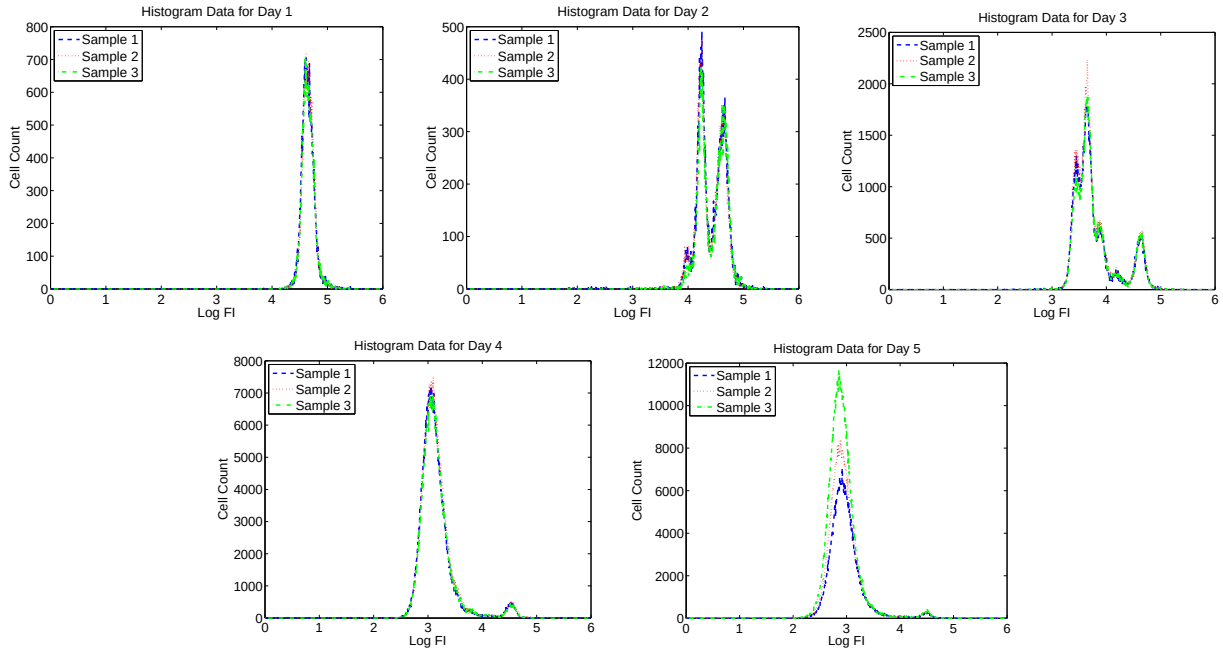

Figure 6: Summary histogram data for CD8+ T cells measured for Donor 2 using ViViD dye to exclude dead cells.

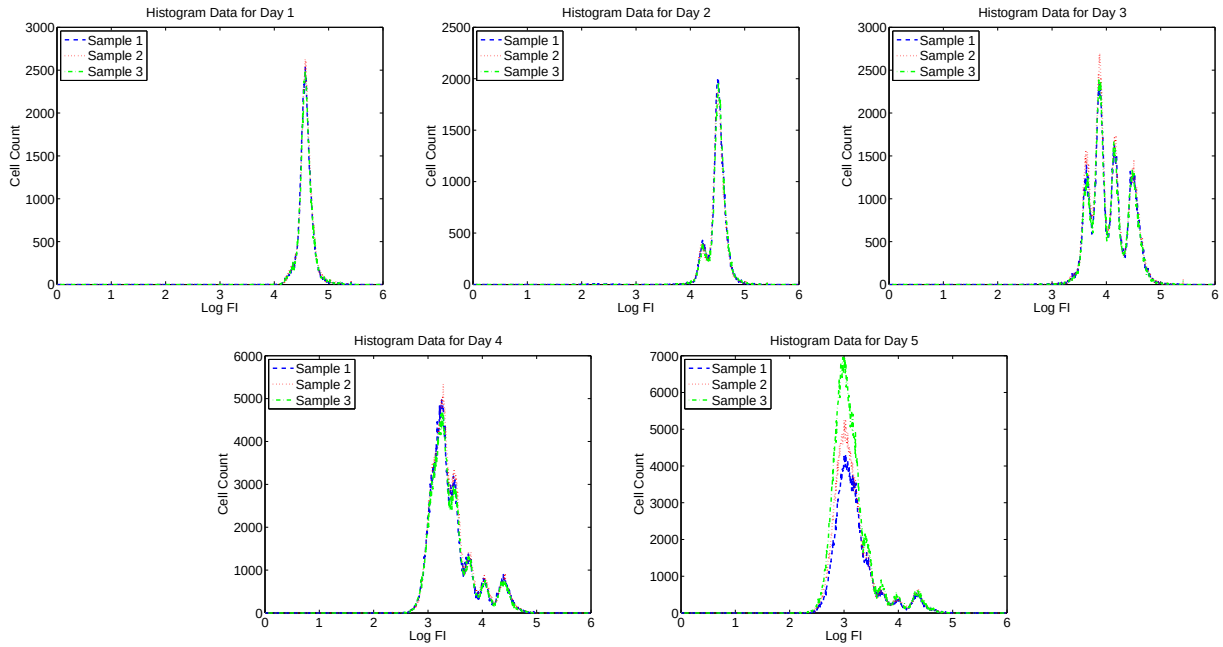

Figure 7: Summary histogram data for CD4+ T cells measured for Donor 2 without using ViViD dye to exclude dead cells.

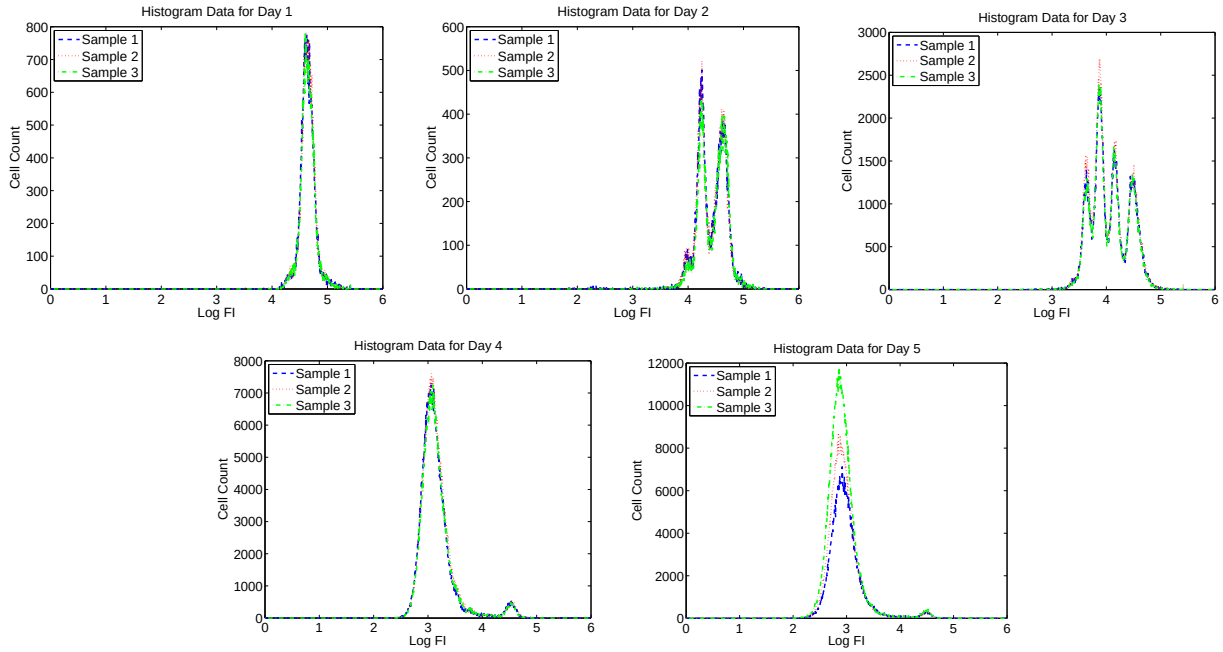

Figure 8: Summary histogram data for CD8+ T cells measured for Donor 2 without using ViViD dye to exclude dead cells.

Chapter 3 of [20]. We remark here that t_0 typically coincides with the time at which the cells were stimulated to divide, but for the purposes of our experiment the first observation actually occurred approximately 24 hours after stimulation. We also mention that the form of the recruitment terms (3.2) assumes an even partitioning of the CFSE in a mother cell between two daughter cells during cytokinesis; i.e., *we assume that each daughter cell receives exactly one half of the CFSE that was present in the mother cell.* Long-standing results indicate that the partitioning of cytoplasm to two daughter cells during mitosis is *not* even [21], and a recent review [9] suggests that incorporating the assumption of asymmetric cell division into mathematical models for cell proliferation will "improve assessment of T cell performance parameters from CFSE-based proliferation assays." Nevertheless, we follow the convention of earlier work [2, 11, 15, 17, 18, 20] in making the simplifying assumption that CFSE is evenly distributed during cell division.

As proposed in [18], the solutions to the system of partial differential equations (PDEs) given in (3.1) can be factored as

$$n_i(t,x) = N_i(t)\bar{n}_i(t,x),$$

where $N_i(t)$ indicates the *number* of cells having completed i divisions at time t and $\bar{n}_i(t,x)$ describes the *distribution* of CFSE within that generation of cells at time t; that is, $\bar{n}_i(t,x)$ is a probability density function (pdf) in the variable x, so that for any fixed t, $\bar{n}_i(t,x) \geq 0$ for all x and

$$\int_0^\infty \bar{n}_i(t,x)\,dx = 1.$$

The N_i's satisfy the system of ordinary differential equations (ODEs) given by

$$\begin{aligned} \frac{dN_0(t)}{dt} &= -(\alpha_0(t)+\beta_0(t))N_0(t) && \text{for } i=0, \\ \frac{dN_i(t)}{dt} &= -(\alpha_i(t)+\beta_i(t))N_i(t) + 2\alpha_{i-1}(t)N_{i-1}(t) && \text{for } i \geq 1, \end{aligned} \tag{3.4}$$

and have initial conditions given by

$$N_i(t_0) = \begin{cases} N_0 = \int_0^\infty \Phi(x)\,dx & \text{for } i=0, \\ 0 & \text{for } i \geq 1. \end{cases} \tag{3.5}$$

Each $\bar{n}_i$ satisfies the PDE

$$\frac{\partial \bar{n}_i(t,x)}{\partial t} - v(t)\frac{\partial [x\bar{n}_i(t,x)]}{\partial x} = 0 \tag{3.6}$$

and the initial condition

$$\bar{n}_i(t_0,x) = \frac{2^i\Phi(2^i x)}{N_0} \tag{3.7}$$

for $x \geq 0$.

It is worth noting that cells will only divide a finite number of times in the time frame of at typical *in vitro* cell culturing experiment. Therefore, we typically compute solutions to (3.4) and (3.6) only for $i \in \{0,1,\ldots,i_{max}\}$, where i_{max} is the largest number of divisions we expect a cell from the initial population to undergo during the period of observation. For a five-day experiment such as that presented in Section 2, it is rare for cells to undergo more than 12 divisions. In order to capture the behavior of all but a negligible number of cells, we use the conservative value of $i_{max} = 16$ for our purposes in this variability study.

3.2 Autofluorescence

Thus far, we have described a model that accounts only for FI *induced by CFSE*, but as noted in [20], the experimentally measured FI of a cell is actually the sum of CFSE-induced FI and the cell's natural "autofluorescence". Therefore, following the work of [11], we let $\tilde{n}_i(t,\tilde{x})$ be a structured density (in cells per unit FI), where i again denotes a specific generation of cells, t denotes time elapsed (in hr), and $\tilde{x}$ denotes *measured* FI. Here,

$$\tilde{x} = x + x_a,$$

where x and x_a represent the FI due to CFSE and autofluorescence, respectively.

If we assume solutions $n_i(t,x)$ to (3.1) and (3.3) have already been computed and that x_a is a realization of a random variable X_a with pdf $f_{X_a}(x_a;t)$, then the densities $\tilde{n}_i(t,\tilde{x})$ can be computed using the convolution integral [11, 18]

$$\tilde{n}_i(t,\tilde{x}) = \int_{-\infty}^{\infty} n_i(t,x) f_{X_a}(\tilde{x}-x;t)\,dx = \int_0^{\tilde{x}} n_i(t,x) f_{X_a}(\tilde{x}-x;t)\,dx. \tag{3.8}$$

Under certain assumptions, this convolution integral can be computed quickly and efficiently as demonstrated in [11].

3.3 Cyton Model for Cell Numbers

We now turn our attention to the cyton model [12, 13], which is an alternative to (3.4) that arises from two simple assumptions. The first, which is self-evident, is that any given cell must eventually either divide or die. The second, which is based upon experimental evidence, is that the processes of cell division and death operate independently of one another [13]. Thus, we can assume that the destiny of any particular cell is governed by two fixed numbers: a "time until division" and a "time until death". In particular, the actual fate of the cell (division or death) can be determined by observing which of these two numbers is smaller. For individual cells within a population of cells sharing similar characteristics (e.g., cells of the same type having undergone the same number of divisions), it is reasonable to assume that the "time until division" and "time until death" are realizations of independent random variables. These random variables are described by probability distributions, and so the cyton model requires parameters that can be used to uniquely determine the probability distributions for times until division and death of cells in a given population (e.g., CD4+ T cells having undergone 1 division). The authors of [13] chose the term "cyton" to denote the "combination of independent cellular machines governing times to divide and die" and represented a cyton mathematically using a pair of probability density functions. For example, if ϕ_i and ψ_i are the pdfs for time until division and time until death, respectively, of cells in generation i, then the cyton for generation i can be denoted (ϕ_i, ψ_i). One additional consideration is that, in reality, not all cells in a given population will divide if they avoid death (at least not within the time frame of a typical *in vitro* cell culturing experiment) [13]. Therefore, the cyton model includes the notion of "progressor fraction": for a given generation of cells, only a certain proportion have the potential to "progress" to the next generation via cell division.

Let F_i denote the progressor fraction for generation i; that is, F_i represents the proportion of cells in generation i that would (eventually) divide in the absence of any possibility of cell death. Then, define the random variable T_i^{div} to be the time required for a cell in generation i (with the *potential* to progress) to complete its next division (measured in hours since the completion of the i^{th} division, or in the case of T_0^{div}, hours since t_0). Similarly, define the random variable T_i^{die} to be the time required for a cell in generation i to die. Finally, let $\phi_i(t)$ and $\psi_i(t)$ be pdfs for T_i^{div} and T_i^{die}, respectively. If we define $N_i(t)$ as before, the cyton model is then given by

$$\begin{aligned} N_0(t) &= N_0 - \int_{t_0}^{t} \left(n_0^{div}(s) + n_0^{die}(s)\right)\,ds \qquad \text{for } i=0, \\ N_i(t) &= \int_{t_0}^{t} \left(2n_{i-1}^{div}(s) - n_i^{div}(s) - n_i^{die}(s)\right)\,ds \quad \text{for } i \geq 1, \end{aligned} \tag{3.9}$$

where $n_i^{div}(t)$ and $n_i^{die}(t)$ are rates (in cells/hr) at which cells in generation i divide and die, respectively. These rates are defined as

$$n_i^{div}(t) = \begin{cases} F_0 N_0 \left(1 - \displaystyle\int_{t_0}^{t} \psi_0(s)\,ds\right) \phi_0(t) & \text{for } i=0, \\ 2F_i \displaystyle\int_{t_0}^{t} n_{i-1}^{div}(s) \left(1 - \int_0^{t-s} \psi_i(\xi)\,d\xi\right) \phi_i(t-s)\,ds & \text{for } i \geq 1. \end{cases} \tag{3.10}$$

and

$$n_i^{die}(t) = \begin{cases} N_0 \left(1 - F_0 \int_{t_0}^{t} \phi_0(s)ds\right) \psi_0(t) & \text{for } i = 0, \\ 2 \int_{t_0}^{t} n_{i-1}^{div}(s) \left(1 - F_i \int_0^{t-s} \phi_i(\xi)\, d\xi\right) \psi_i(t-s)\, ds & \text{for } i \geq 1. \end{cases} \tag{3.11}$$

There is considerable experimental evidence [7, 12, 13] that supports the cyton model, and it has an advantage over models such as (3.4) in that it directly connects cell population numbers to probablity distributions describing times at which cells in a given generation will divide or die. Identifying these distributions for populations of lymphocytes exposed to specific environmental stimuli allows for a detailed quantitative description of the adaptive immune response.

3.4 Label-Structured Cyton Model for Cell Densities

As in [2], we incorporate the cyton model for cell numbers into the division- and label-structured model framework described previously by replacing the sink and source terms in the right-hand sides of (3.1) with terms involving the cyton-based rates to obtain

$$\begin{aligned} \frac{\partial n_0(t,x)}{\partial t} - v(t)\frac{\partial [x n_0(t,x)]}{\partial x} &= -(n_0^{div}(t) + n_0^{die}(t))\bar{n}_0(t,x) && \text{for } i = 0, \\ \frac{\partial n_i(t,x)}{\partial t} - v(t)\frac{\partial [x n_i(t,x)]}{\partial x} &= (2n_{i-1}^{div}(t) - n_i^{div}(t) - n_i^{die}(t))\bar{n}_i(t,x) && \text{for } i \geq 1. \end{aligned} \tag{3.12}$$

Solutions of this system are then given by $n_i(t,x) = N_i(t)\bar{n}_i(t,x)$, where the $N_i(t)$'s satisfy the cyton model equations (3.9) and initial conditions (3.5) and each $\bar{n}_i(t,x)$ satisfies (3.6) and (3.7) as before.

Like (3.1), the model given by (3.12) may be properly described as a division- and label-structured population model, as it makes use of structure variables for division number (or generation) i and CFSE label content (which is proportional to CFSE-wavelength FI) x. Also, as described in [11, 18] and summarized in [2], the factorable form of the solutions $\{n_i(t,x)\}$ and the technique for converting these to corresponding solutions $\{\tilde{n}_i(t,\tilde{x})\}$ via convolution integrals (cf. (3.8)) makes it possible to obtain numerical solutions very quickly when the model parameters are given [2, 11]. This model has been shown to yield a reasonably good fit to summary histogram data such as that presented in Figures 1 through 8, provided that the model parameters are chosen "optimally" [2]. More will be said about optimal parameter estimation in Section 4.

Finally, we remark that (3.12) actually describes an entire class of models. In order to specify a particular model for further investigation, we must decide on forms for the distribution of the autofluorescence X_a, the (exponential) label decay rate $v(t)$, the cytons $\{(\phi_i(t), \psi_i(t))\}$, and the progressor fractions $\{F_i\}$.

3.5 Parameterization for a Specific Mathematical Model

Here, we list the assumptions for the specific cyton-based mathematical model we consider and describe the parameters that we use to designate this model. All of the parameters for our specific mathematical model are provided in Table 1.

First, we assume that the random variable X_a is time-independent and has a lognormal distribution with mean and variance denoted $\mathrm{E}[X_a]$ and $\mathrm{Var}[X_a]$, respectively. Although experiments indicate that the distribution of autofluorescence does, in fact, vary with time, ignoring this time-dependence greatly reduces the number of parameters required to designate the model and still allows for a reasonable fit to summary histogram data [2]. We therefore have two parameters that completely describe the distribution of autofluorescence: $\mathrm{E}[X_a]$ and $\mathrm{SD}[X_a] = (\mathrm{Var}[X_a])^{1/2}$, which are listed as parameters (1) and (2), respectively, in Table 1.

Next, we assume that the rate of decay in CFSE-induced FI is given by $v(t) = c$, where $c > 0$ is some constant. This follows the convention of [2], in which the authors assume that an exponential decay model is sufficient to describe decay of CFSE in experiments for which *the first data collection time occurs after approximately 24 hours*. We note that the decay of intracellular CFSE has been observed to occur very rapidly during the first 24 hours after initial labeling and much slower thereafter [5, 20] and that this

observation can be fully supported with molecular-level modeling [1]. Thus, when data are collected in the first 24 hours, it is more accurate to describe the rate of loss of fluorescence intensity with a time-varying rate, as in a Gompertz decay model. For our situation, however, we require only one parameter to completely describe the decay of CFSE: c, which is listed as parameter (3) in the aforementioned table.

We assume that each T_i^{div} has a lognormal distribution with mean and variance denoted $\mathrm{E}\left[T_i^{div}\right]$ and $\mathrm{Var}\left[T_i^{div}\right]$, respectively. We further assume that, for $i \geq 1$, all T_i^{div} are independent and identically distributed (*i.i.d.*). Such assumptions are consistent with earlier work using the cyton model [2, 12, 13]. We therefore have four parameters that completely describe $\{T_i^{div}\}$: $\mathrm{E}\left[T_0^{div}\right]$, $\mathrm{SD}\left[T_0^{div}\right] = (\mathrm{Var}\left[T_0^{div}\right])^{1/2}$, $\mathrm{E}\left[T^{div}\right] = \mathrm{E}\left[T_i^{div}\right]$ for $i \geq 1$, and $\mathrm{SD}\left[T^{div}\right] = \mathrm{SD}\left[T_i^{div}\right] = (\mathrm{Var}\left[T_i^{div}\right])^{1/2}$ for $i \geq 1$. These are listed as parameters (4) through (7), respectively.

We also assume that the random variables T_i^{die} for $i \geq 1$ are *i.i.d.* with a lognormal distribution, in this case with mean and variance denoted $\mathrm{E}\left[T^{die}\right]$ and $\mathrm{Var}\left[T^{die}\right]$, respectively. Again such assumptions are consistent with earlier work [2, 12, 13]. We further assume that there is no death for undivided cells (i.e., those cells in generation $i = 0$). In reality, there tends to be a large die-off of cells following stimulation with PHA [6], but we reiterate that for this report the first data were collected approximately 24 hours post-stimulation. As a result, *the initial conditions for our mathematical model only reflect those cells that have not died in the first 24 hours after stimulation.* Therefore, as in [2], we work under the assumption that the cells in our "initial population" (consisting of those undivided cells that are still alive 24 hours after stimulation) that do not go on to divide experience essentially no death for the duration of the experiment. Hence, we have two parameters that completely describe $\{T_i^{die}\}$: $\mathrm{E}\left[T^{die}\right] = \mathrm{E}\left[T_i^{die}\right]$ and $\mathrm{SD}\left[T^{die}\right] = \mathrm{SD}\left[T_i^{die}\right] = (\mathrm{Var}\left[T_i^{die}\right])^{1/2}$ for $i \geq 1$, which are listed as parameters (7) and (8), respectively.

The only remaining parameters that are required to characterize our model are the progressor fractions $\{F_i\}$. We allow F_0 to be one of our required model parameters and assume that each progressor fraction F_i with $i \geq 1$ is uniquely determined by the mean and standard deviation of a "discrete normal distribution", denoted D_μ and D_σ, respectively. This is consistent with the "division destiny" approach for determining progressor fractions that was employed in [13] and [2], and we refer the interested reader to [2] for a complete discussion of the method by which the progressor fractions are computed. We therefore have three parameters that can be used to determine all the progressor fractions: F_0, D_μ, and D_σ, which are listed as parameters (10) through (12), respectively.

Thus, our specific model depends on exactly 12 parameters. We remark that parameters (1) through (3), while important for describing the data, are not considered to be "biologically relevant" parameters in the sense that they do not have any bearing on the proliferative behavior of a population of cells. Also, parameters (4), (6), (8), and (10) are perhaps the most important of the biologically relevant parameters

Number	Parameter	Description
1	$\mathrm{E}[X_a]$	mean autofluorescence
2	$\mathrm{SD}[X_a]$	standard deviation of autofluorescence
3	c	exponential decay rate for CFSE
4	$\mathrm{E}\left[T_0^{div}\right]$	mean time to divide for cells in generation $i = 0$
5	$\mathrm{SD}\left[T_0^{div}\right]$	standard deviation of time to divide for cells in generation $i = 0$
6	$\mathrm{E}\left[T^{div}\right]$	mean time to divide for cells in later generations ($i \geq 1$)
7	$\mathrm{SD}\left[T^{div}\right]$	standard deviation of time to divide for cells in later generations ($i \geq 1$)
8	$\mathrm{E}\left[T^{die}\right]$	mean time to die for cells in later generations ($i \geq 1$)
9	$\mathrm{SD}\left[T^{die}\right]$	standard deviation of time to die for cells in later generations ($i \geq 1$)
10	F_0	progressor fraction for cells in generation $i = 0$
11	D_μ	mean of discrete normal distribution (used to compute F_i for $i \geq 1$)
12	D_σ	standard deviation of discrete normal distribution (used to compute F_i for $i \geq 1$)

Table 1: Parameters for specific mathematical model.

because their interpretation in the context of cell proliferation is the most straightforward. Note that the specific cyton-based model described here is denoted Model 6 (with exponential label decay) in [2].

4 Parameter Estimation

In order to estimate the parameters in our specific mathematical model, we must first describe a statistical model that relates observable data to the mathematical model. As was previously explained, CFSE flow cytometry data are typically summarized in the form of histograms, and furthermore, measured FI is commonly represented on a logarithmic scale (cf. Figures 1 through 8). Therefore, we begin by describing how our model can be used to obtain information on cell numbers in a form that can be compared directly with such summarized experimental data.

If we define the structured densities $\tilde{n}_i(t,\tilde{x})$ (in terms of *measured* FI) as in Section 3, then the structured density for the entire population of cells is

$$\tilde{n}(t,\tilde{x}) = \sum_{i=0}^{\infty} \tilde{n}_i(t,\tilde{x}) \approx \sum_{i=0}^{i_{max}} \tilde{n}_i(t,\tilde{x}).$$

(See Section 3.1 for a discussion of how to choose i_{max} appropriately.) Now, because CFSE histogram data are most commonly reported using a base 10 logarithmic scale, we let $z = \log_{10}(\tilde{x})$ so that

$$\hat{n}(t,z) = 10^z \log(10)\, \tilde{n}(t,10^z)$$

gives the structured density in cells per base 10 log unit FI.

In the discussion that follows, we let $\vec{q}_0$ denote a hypothetical "true" parameter vector (so that, in the case of our specific mathematical model, $\vec{q}_0 \in \mathbb{R}^{12}$) and let

$$I[\hat{n}](t_j,z_k;\vec{q}_0) = \int_{z_k}^{z_{k+1}} \hat{n}(t_j,z;\vec{q}_0)\, dz \tag{4.1}$$

denote the total number of cells with log (base 10) FI in the interval $[z_k, z_{k+1}]$ at time t_j. Also, we let B denote the (fixed) total number of beads in each sample tube and b_j denote the number of beads counted for the sample measured at time t_j.

Now, let N_k^j be a random variable representing the number of cells with log FI in the interval $[z_k, z_{k+1})$ measured at time t_j. Then it has been argued [2] that

$$N_k^j \sim \mathcal{N}\left(I[\hat{n}](t_j,z_k;\vec{q}_0), \frac{B}{b_j} I[\hat{n}](t_j,z_k;\vec{q}_0) \right); \tag{4.2}$$

i.e., each N_k^j is normally distributed with mean $I[\hat{n}](t_j,z_k;\vec{q}_0)$ and variance $\frac{B}{b_j} I[\hat{n}](t_j,z_k;\vec{q}_0)$. Note that this does not lead to either (1) a constant variance model or (2) a constant coefficient of variance model. Though these latter two types of statistical models are commonly assumed to underly data-collection processes [8, 10, 19], modified residual plots indicate that (4.2) is a better choice in this case [4, 20].

Define the weighted least squares (WLS) parameter *estimator*

$$\vec{q}_{WLS} = \arg\min_{\vec{q}\in Q} J(\vec{q};\{N_k^j\}),$$

where

$$J(\vec{q};\{N_k^j\}) = \sum_{j,k} \frac{(I[\hat{n}](t_j,z_k;\vec{q}) - N_k^j)^2}{w_k^j},$$

Q denotes the space of allowable parameter vectors, and the *weights* (selected to match the variance of the N_k^j's) are given by

$$w_k^j = \begin{cases} \frac{B}{b_j} I[\hat{n}](t_j,z_k;\vec{q}_0) & \text{for } I[\hat{n}](t_j,z_k;\vec{q}_0) > I^*, \\ \frac{B}{b_j} I^* & \text{for } I[\hat{n}](t_j,z_k;\vec{q}_0) \le I^*. \end{cases} \tag{4.3}$$

The value of I^* is positive to prevent division by zero, and in practice it is selected such that the modified residual plots produce uniform random patterns. We once again follow the convention of [2] and set $I^* = 200$.

If we consider the measured data to be a set of realizations $\{n_k^j\}$ of the random variables $\{N_k^j\}$, we can obtain the WLS parameter *estimate*

$$\hat{q}_{WLS} = \arg\min_{\vec{q}\in Q} J(\vec{q}; \{n_k^j\}). \tag{4.4}$$

Note that to compute the weights $\{w_k^j\}$ we need $\vec{q}_0$, but to estimate $\vec{q}_0$ we need the weights. In order to overcome this obstacle, we use a conventional weighted least squares iterative estimation procedure [8] as described in Algorithm 4.1. In this algorithm, note that ε is a threshold tolerance that allows the user to specify a termination criterion, $\vec{q}_{typ}$ is a vector with elements that reflect the relative sizes of the parameters to be estimated, and "./" denotes element-wise division.

Algorithm 4.1 Parameter Estimation Procedure

1. Obtain initial estimate $\hat{q}^{(0)}$ using (4.4) with $w_k^j = 1$ for all j, k.
2. Compute weights w_k^j using (4.3) with $\vec{q}_0$ replaced by $\hat{q}^{(0)}$.
3. Initialize the iteration counter ℓ with the value 1.
4. Do each of the following:
   - Compute $\hat{q}^{(\ell)}$ using (4.4) with current weights w_k^j.
   - Update the weights using (4.3) with $\vec{q}_0$ replaced by $\hat{q}^{(\ell)}$.
   - Store the value of $\left|\left|[\hat{q}^{(\ell)} - \hat{q}^{(\ell-1)}]./[\vec{q}_{typ}]\right|\right|$ in Δ.
   - Increment ℓ by 1.
5. If $\Delta > \varepsilon$, return to Step 4. Otherwise, terminate the algorithm.

5 Results and Discussion

In this section, we discuss the results of our study. Since triplicate measurements were collected at each point in a five-day time series, we are able to analyze the variability that exists in the data itself. Also, since these triplicate measurements make it possible to construct a large number of five-day data sets, we are able to analyze variability in the corresponding sets of parameter estimates. We consider experimental variability in the estimates for individual parameters (for each specific combination of donor, ViViD dye status, and cell type) as well as biological variability (i.e., differences between the parameter estimates obtained for different donors and different cell types).

5.1 Variability in the Data

It is clear from Figures 1 through 8 that, while the *shapes* of the histograms summarizing observed data do not vary much between triplicate experiments for any particular day and combination of donor, ViViD dye status, and cell type, the *scale* of the histograms can vary considerably. That is, there can be a significant difference between triplicate experiments in the *number* of cells represented in the respective histograms. One can also see in Figures 1 through 8 that there seems to be more variability in the cell counts at the later time points (those corresponding to Day 4 and especially those corresponding to Day 5). Tables 2 through 6 list the cell counts for each sample and each combination of donor, ViViD dye status, and cell type on Days 1 through 5, respectively, and can be compared with the histograms in Figures 1 through 8. For example, Table 2 shows all the cell counts in the various samples represented in the upper-left (Day 1) plots for each

of Figures 1 through 8. Tables 2 through 6 also show an estimate of the coefficient of variation based on each row of sample cell counts. The coefficient of variation is a measure of the relative variation in the cell counts, and can be estimated as

$$\hat{c}_v = \frac{s}{\bar{x}},$$

where $\bar{x}$ denotes the sample mean of the cell counts (in the relevant biological samples) and s denotes the sample standard deviation. We refer to $\hat{c}_v$ as an "estimate" because it is derived from a finite "sample" of data (in our case, from three cell counts derived from three biological samples). The true coefficient of variation would be computed as

$$c_v = \frac{\sigma}{\mu},$$

where μ and σ are the mean and standard deviation, respectively, of cell counts for the "population" of all possible biological samples for the specific time, donor, ViViD status, and cell type in question.

In order to understand how variation in the cell counts arises, recall from Section 2 that *approximately* 1 million cells were placed into each of several wells, and that each distinct sample was drawn from a distinct well. Because of the experimental error inherent in seeding the wells, we expect that each well actually started out with a different number of cells. We should remark here that the numbers in Tables 2 through 6 do not represent total cell counts, but rather they represent cell counts for specific types of cells (CD4+ or CD8+ T cells) under specific conditions (donor and ViViD dye status). So, for example, if we attempt to seed 1 million cells from Donor 1 into a well and the true proportion of CD4+ T cells is 15% for this donor, there should be about 150 thousand CD4+ T cells in the well at time $t = 0$; however, there will be some variation in this number (150 thousand) because of the variation in the total cell population number (1 million). We did not make any measurements at time $t = 0$, so we cannot directly assess the variation present in the numbers of cells initially seeded into the wells. Our best approximation of this initial variation comes from the cell counts observed on Day 1, which are shown in Table 2. Also, because the true proportion of cells (out of approximately 1 million) corresponding to a particular day, donor, ViViD dye status, and cell type varies, we cannot directly compare all 24 cell count numbers in one of the tables, and we cannot directly compare the 8 *sample variances* or *sample standard deviations* obtained for the 8 rows in any given table. To be clear, we cannot use such direct comparisons because the *magnitudes* of the cell count numbers tend to be different in each row of a given table. We can, however, compare some measure of *relative* variation for each of the rows of a given table. The coefficient of variation described previously is one such measure. So, the 8 numbers listed in the last column of Table 2 give some indication of the variability we expect when attempting to seed 1 million cells into a well, and, importantly, they can be compared with one another.

If we assume that the seeding of 1 million cells into a well is a process that is subject to random error, then the amount of error is a random variable with some well-defined probability distribution. For our purposes, the "amount of error in the initial seeding" is synonymous with the "amount of relative variation in the cell counts at Day 1", which we choose to measure using the coefficients of variation described previously. One important question to consider, then, is whether or not the amount of relative variation in cell counts (or more precisely, the sampling distribution of this statistic) changes between measurement times (days). As was previously asserted, Figures 1 through 8 provide convincing evidence that the amount of relative variation in cell counts does change with respect to time. More specifically, these figures lead us to suspect that there is a significant difference between the relative variation observed in the earlier days of the experiment (1 through 3) and that observed in the later days (4 and 5). The coefficient of variation estimates in the last columns of Tables 2 through 6 can be used to demonstrate this claim conclusively through the use of formal statistical hypothesis testing.

The two-sided Wilcoxon rank-sum test allows one to determine if two independent samples have been drawn from the same continuous distribution [14]. In our case, we assume that the eight coefficient of variation numbers corresponding to Day i are a random sample of a continuous random variable with cumulative density function (cdf) F_i for $i \in \{1, 2, 3, 4, 5\}$ and that each of the five samples is independent of all of the others. Thus, for any particular pair of days (i, j), we would like to test the null hypothesis that the corresponding samples of coefficient of variation numbers were drawn from the same population of

Donor	ViViD Used	Cell Type	Sample 1	Sample 2	Sample 3	C.V.
1	Y	CD4	104124	117820	122408	8.29%
1	Y	CD8	36778	38924	40190	4.47%
1	N	CD4	128161	140770	146369	6.74%
1	N	CD8	39899	42259	43478	4.34%
2	Y	CD4	68651	68439	68680	0.19%
2	Y	CD8	28699	28574	27387	2.57%
2	N	CD4	91542	95914	90740	3.00%
2	N	CD8	33983	34605	32692	2.89%

Table 2: Status of cell cultures at Day 1. The numbers in the columns corresponding to Samples 1, 2, and 3 represent cell counts after scaling (using bead counts). Each number in the C.V. column represents the coefficient of variation for the cell counts in the corresponding row.

Donor	ViViD Used	Cell Type	Sample 1	Sample 2	Sample 3	C.V.
1	Y	CD4	128535	139264	149408	7.51%
1	Y	CD8	58115	61406	67116	7.32%
1	N	CD4	156211	171078	181924	7.61%
1	N	CD8	70147	75010	82658	8.31%
2	Y	CD4	66884	63458	63162	3.21%
2	Y	CD8	29242	28221	26734	4.49%
2	N	CD4	82968	80701	80098	1.86%
2	N	CD8	33223	33107	31048	3.77%

Table 3: Status of cell cultures at Day 2. The numbers in the columns corresponding to Samples 1, 2, and 3 represent cell counts after scaling (using bead counts). Each number in the C.V. column represents the coefficient of variation for the cell counts in the corresponding row.

Donor	ViViD Used	Cell Type	Sample 1	Sample 2	Sample 3	C.V.
1	Y	CD4	278399	277201	269793	1.69%
1	Y	CD8	190473	183328	179769	2.95%
1	N	CD4	331038	338423	328589	1.54%
1	N	CD8	232513	228392	228203	1.06%
2	Y	CD4	187718	206164	184355	6.09%
2	Y	CD8	137646	150831	136055	5.73%
2	N	CD4	212391	229784	208054	5.31%
2	N	CD8	145740	158148	143890	5.19%

Table 4: Status of cell cultures at Day 3. The numbers in the columns corresponding to Samples 1, 2, and 3 represent cell counts after scaling (using bead counts). Each number in the C.V. column represents the coefficient of variation for the cell counts in the corresponding row.

Donor	ViViD Used	Cell Type	Sample 1	Sample 2	Sample 3	C.V.
1	Y	CD4	746988	611600	N/A	14.09%
1	Y	CD8	778452	616165	N/A	16.46%
1	N	CD4	813670	672320	N/A	13.45%
1	N	CD8	845757	672287	N/A	16.16%
2	Y	CD4	465445	495995	450620	4.92%
2	Y	CD8	562295	596485	550758	4.17%
2	N	CD4	483623	512917	466908	4.77%
2	N	CD8	572560	606627	560635	4.12%

Table 5: Status of cell cultures at Day 4. The numbers in the columns corresponding to Samples 1, 2, and 3 represent cell counts after scaling (using bead counts). Each number in the C.V. column represents the coefficient of variation for the cell counts in the corresponding row.

Donor	ViViD Used	Cell Type	Sample 1	Sample 2	Sample 3	C.V.
1	Y	CD4	675662	703755	731910	4.00%
1	Y	CD8	960299	763048	823195	11.91%
1	N	CD4	755566	752181	780992	2.06%
1	N	CD8	998167	794116	853743	11.90%
2	Y	CD4	418710	500372	659604	23.28%
2	Y	CD8	578203	700480	940572	24.92%
2	N	CD4	435902	519138	678801	22.67%
2	N	CD8	590954	712185	954256	24.58%

Table 6: Status of cell cultures at Day 5. The numbers in the columns corresponding to Samples 1, 2, and 3 represent cell counts after scaling (using bead counts). Each number in the C.V. column represents the coefficient of variation for the cell counts in the corresponding row.

values (or, equivalently, from two populations with identical cdfs); i.e.,

$$H_0 : F_i(x) = F_j(x) \text{ for all } x.$$

For the Wilcoxon test, the alternative hypothesis is that one of the two samples was drawn from a population that tends to have larger values than the population from which the other sample was drawn (or, equivalently, that one of the two corresponding distributions is *stochastically larger* than the other); i.e.,

$$\begin{aligned} H_A : \quad & F_i(x) \leq F_j(x) \text{ for all } x, \text{ with strict inequality for at least some } x, \\ & \text{or } F_i(x) \geq F_j(x) \text{ for all } x, \text{ with strict inequality for at least some } x. \end{aligned}$$

As with any statistical hypothesis test, the Wilcoxon test produces a "test statistic" that can be converted into a "p-value". The p-value indicates the probability of obtaining a test statistic at least as extreme as the one which was actually observed *assuming that the null hypothesis is true*. If we use a "significance level" of 0.05, then we are asserting that outcomes with probability less than 0.05 are unlikely to occur. Therefore, we should reject the null hypothesis whenever the p-value is less than 0.05.

Suppose, for example, that we want to test the claim that there is no difference between the distribution of relative variations in cell counts observed at Day 1 and that observed at Day 2. This null hypothesis can be formalized as

$$H_0 : F_1(x) = F_2(x) \text{ for all } x,$$

where F_1 and F_2 denote the cdfs for the coefficients of variation in cell counts at Days 1 and 2, respectively.

The alternative hypothesis is that one of the two distributions is *stochastically larger* than the other; i.e.,

$$\begin{aligned} H_A: \quad & F_1(x) \leq F_2(x) \text{ for all } x, \text{ with strict inequality for at least some } x, \\ & \text{or } F_1(x) \geq F_2(x) \text{ for all } x, \text{ with strict inequality for at least some } x. \end{aligned}$$

We can use the coefficient of variation estimates from Tables 2 and 3 to perform a Wilcoxon test for these hypotheses. That is, we can compare the eight coefficient of variation numbers from Table 2 with the eight coefficient of variation numbers from Table 3 using a Wilcoxon test. Based on the p-value of 0.2345 that results from performing this test, we fail to reject the null hypothesis (using a 0.05 significance level) and conclude that there is not a statistically significant difference between the relative variations in cell counts observed at Days 1 and 2, respectively. Similarly, we can perform Wilcoxon tests to conclude that there is not a statistically significant difference between the relative variations in cell counts observed at Days 1 and 3 ($p = 0.8785$) or the relative variations in cell counts observed at Days 2 and 3 ($p = 0.1304$). On the other hand, Wilcoxon tests lead us to conclude that there *is* a statistically significant difference between the relative variations in cell counts observed at Days 1 and 4 ($p = 0.03792$) and between the relative variations in cell counts observed at Days 1 and 5 ($p = 0.02813$). Similarly, there appears to be a statistically significant difference between the relative variations in cell counts observed at Days 2 and 5 ($p = 0.03792$) and between the relative variations in cell counts observed at Days 3 and 5 ($p = 0.01476$). (Wilcoxon tests do not indicate a significant difference between relative variations in cell counts observed at Days 2 and 4 or Days 3 and 4, but recall that at least some of the Day 4 coefficients of variation are based on fewer cell counts because fewer biological samples were used for Donor 1 on Day 4; therefore, information concerning variation in cell counts for Day 4 is considerably less reliable.)

We propose that this change in the relative variation of the cell counts with respect to time cannot be explained by proliferation dynamics. In fact, if we assume that our mathematical model describing cell proliferation is correct, the relative variation in cell counts for distinct cultures proliferating with the same dynamics should not change in time. Relative variation can be measured in terms of percent differences or coefficients of variation and we offer proofs of the assertion in the preceding sentence with respect to both of these measures of relative variation in Appendix A of [3], but it is easy (and instructive) to understand the validity of the assertion under the assumption of a simple exponential growth model. So, consider two cultures of cells, "A" and "B", that are proliferating at the same exponential growth rate α. If A_0 and B_0 denote the initial numbers of cells present in cultures A and B, respectively, then

$$A(t) = A_0 e^{\alpha t}$$

and

$$B(t) = B_0 e^{\alpha t}$$

describe the numbers of cells in the respective cultures at time t. The initial percent difference in the cell counts is

$$\frac{2(A_0 - B_0)}{A_0 + B_0},$$

while the percent difference at any later time t is also

$$\frac{2(A_0 e^{\alpha t} - B_0 e^{\alpha t})}{A_0 e^{\alpha t} + B_0 e^{\alpha t}} = \frac{2(A_0 - B_0)e^{\alpha t}}{(A_0 + B_0)e^{\alpha t}} = \frac{2(A_0 - B_0)}{A_0 + B_0}.$$

Therefore, the percent difference in cell counts does not change with respect to time. Note that the amount of statistical *variation* (e.g., difference) in the cell counts *does* generally change in time, but the *relative variation* (e.g., percent difference) must remain constant.

Since we have clearly demonstrated that the relative variation in the cell counts does, indeed, change between Days 1, 2, and 3 and Day 5, then some source of variability must exist which is not accounted for in our model. We propose that the exchange of nutrient medium starting at Day 3 could be such a source of variability. Exchange of nutrient medium could feasibly remove, disturb, or damage some of the cells in the affected wells, and it would certainly change the amount of nutrient available to the cells in

those wells. In fact, *the very reason that the nutrient medium is replenished starting at Day 3 is that by that time it has begun to change color, indicating that the nutrient levels have declined.* So, in addition to the changes in the amount of nutrient available to the cell cultures that occur at discrete points in time corresponding to nutrient medium exchange, we may infer that cells growing and dividing in the various cell cultures significantly deplete nutrients in their respective wells *throughout the experiment.*

5.2 Variability in the Parameter Estimates

In order to assess variability in parameter estimates, we applied the parameter estimation technique described in Section 4 to the various five-day time series data sets described in Section 2. For each of the 12 parameters from our specific mathematical model and each of the eight combinations of donor ("Donor1" or "Donor2"), ViViD dye status ("Vivid" indicating that ViViD dye was used to exclude dead cells or "NoVivid" indicating otherwise), and cell type ("CD4" or "CD8"), this led to either 162 or 243 (depending on donor, cf. Section 2) parameter estimates. Each such set of parameter estimates can be represented by a box plot, so for each model parameter we can construct eight box plots. To illustrate this we provide Figure 9, which shows the parameter estimation results for the model parameters c and $\mathrm{E}\left[T^{die}\right]$ for each combination of donor, ViViD dye status, and cell type. The box plots in this figure adhere to the following conventions: (i) the median value is indicated by a red line; (ii) the first and third quartiles (Q_1 and Q_3) are indicated by the lower and upper boundaries of the blue box, respectively; (iii) any value that falls above $Q_3 + 1.5(Q_3 - Q_1)$ or below $Q_1 - 1.5(Q_3 - Q_1)$ is considered to be an outlier, and is indicated by a "+"; and (iv) the black horizontal lines above and below the box (which are in most cases connected to the box via dashed vertical lines) represent the maximimum and minimum values, respectively, excluding outliers.

Sets of box plots such as those described above can provide a wealth of information concerning the variability in parameter estimates and identifiability of the corresponding parameters. Individually, each box plot can be used to determine a median parameter estimate and to visualize the variation (spread) in parameter estimates for a given donor and cell type when multiple five-day data sets are considered. The amount of spread in each box plot can also be used to conclude whether or not a particular parameter is likely to be identifiable for any particular donor and cell type. For example, Figure 9 reveals extremely large spreads in many of the box plots corresponding to the parameter $\mathrm{E}\left[T^{die}\right]$, indicating that this model parameter may not be identifiable. On the other hand, all of the box plots corresponding to the parameter c have relatively small spreads, indicating that this model parameter can be estimated with relatively high reliability.

Taken together, all the box plots corresponding to a given parameter allow for useful comparisons of the parameter estimates that are obtained for different combinations of donor, vivid dye status, and cell type. For example, if we consider the box plots in Figure 9 corresponding to the parameter c, we can make a number of interesting conclusions. First, the use of ViViD dye does not appear to lead to a statistically significant difference in the estimate obtained for the parameter c (cf. box plots 1 and 3, 2 and 4, 5 and 7, and 6 and 8, numbering sequentially from left to right). Next, the estimate for c is larger for CD8+ T cells than for CD4+ T cells when considering data for Donor 1 (cf. box plots 1 and 2 or 3 and 4), but it is larger for CD4+ T cells than for CD8+ T cells when considering data for Donor 2 (cf. box plots 5 and 6 or 7 and 8). Finally, while there does not appear to be a statistically significant difference between Donor 1 and Donor 2 in the estimate obtained for c when considering CD4+ T cells (cf. box plots 1 and 5 or 3 and 7), the Donor 1 estimate is considerably larger than the Donor 2 estimate when considering CD8+ T cells (cf. box plots 2 and 6 or 4 and 8).

5.2.1 Remarks on Basic Parameter Estimates

We next summarize all the conclusions that can be drawn by analyzing box plots corresponding to parameter estimates for all 12 of our model parameters. In Figure 9, we only show box plots for the parameters c and $\mathrm{E}\left[T^{die}\right]$, but the interested reader can find box plots for all 12 parameters in Figures 9 through 20 of [3]. One general conclusion that can be made from these figures is that the use of ViViD dye does not seem to have a large effect on the estimates obtained for most of the model parameters. Therefore, in the discussion that follows we will focus on the box plots summarizing "NoVivid" data sets.

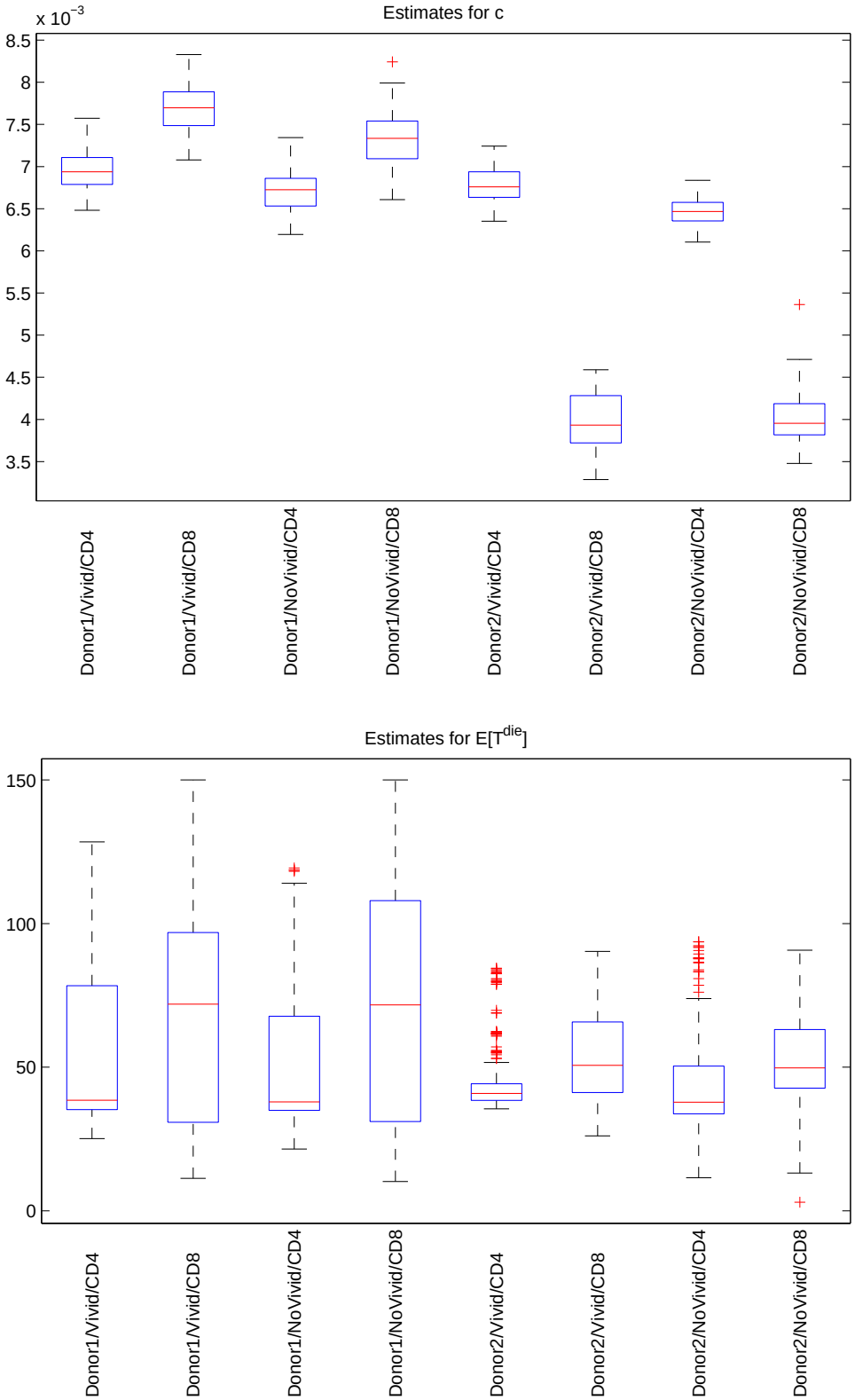

Figure 9: Box plots illustrating variability in estimates for the parameters c (top) and $\mathrm{E}\left[T^{die}\right]$ (bottom).

Box plots summarizing estimates for the parameter $\mathrm{E}[X_a]$, which represents the mean autofluorescence, are shown in Figure 9 of [3]. The 3rd and 4th box plots in that figure indicate that there is a considerable difference in the mean autofluorescence of CD4+ T cells and CD8+ T cells obtained from Donor 1. (Note that the box plots do not "overlap".) More specifically, CD8+ T cells appear to have a larger mean autofluorescence than CD4+ T cells for Donor 1. On the other hand, the 7th and 8th box plots indicate that CD4+ T cells have a larger mean autofluorescence than CD8+ T cells when considering cells obtained from Donor 2. When we compare CD4+ T cells obtained from the two distinct donors (compare 3rd and 7th box plots), it appears that $\mathrm{E}[X_a]$ is larger for Donor 2 than for Donor 1. When comparing CD8+ T cells from the two donors (compare 4th and 8th box plots), it appears that $\mathrm{E}[X_a]$ is larger for Donor 1 than for Donor 2.

In Figure 10 of [3], we provide box plots summarizing estimates for standard deviation of the autofluorescence, $\mathrm{SD}[X_a]$. As with the mean autofluorescence, it appears that the value of this parameter is larger for CD8+ T cells than for CD4+ T cells in the case of Donor 1 and larger for CD4+ T cells than for CD8+ T cells in the case of Donor 2. Also, when comparing CD4+ T cells obtained from the two distinct donors, it appears that $\mathrm{SD}[X_a]$ is larger for Donor 2 than for Donor 1, and when comparing CD8+ T cells from the two donors, it appears that $\mathrm{SD}[X_a]$ is larger for Donor 1 than for Donor 2.

Box plots summarizing estimates for the parameter c, which describes exponential decay of CFSE, are shown in Figure 11 of [3]. It appears that the value of this parameter is larger for CD8+ T cells than for CD4+ T cells in the case of Donor 1 and larger for CD4+ T cells than for CD8+ T cells in the case of Donor 2. When we compare CD4+ T cells obtained from the two distinct donors, there does not appear to be a significant difference in the parameter c; however, when comparing CD8+ T cells from the two donors, it appears that c is larger for Donor 1 than for Donor 2.

In Figure 12 of [3], we provide box plots summarizing estimates for the parameter $\mathrm{E}\left[T_0^{div}\right]$, which represents the mean time to divide for undivided cells. It appears that the value of this parameter is larger for CD4+ T cells than for CD8+ T cells, regardless of which donor we consider. Also, there does not appear to be a significant difference in $\mathrm{E}\left[T_0^{div}\right]$ when comparing CD4+ or CD8+ T cells obtained from the two distinct donors. Figure 13 of [3] indicates that similar statements hold true for $\mathrm{SD}\left[T_0^{div}\right]$, which represents the standard deviation in the time to divide for undivided cells.

Box plots summarizing estimates for the parameter $\mathrm{E}\left[T^{div}\right]$, which represents the mean time to divide for cells that have divided at least once, are shown in Figure 14 of [3]. There does not appear to be a significant difference in the value of this parameter for CD4+ and CD8+ T cells, whether we consider cells from Donor 1 or Donor 2. On the other hand, when we compare CD4+ or CD8+ T cells from the two distinct donors, it appears that $\mathrm{E}\left[T^{div}\right]$ is larger for Donor 1 than for Donor 2.

In Figure 15 of [3], we provide box plots summarizing estimates for the parameter $\mathrm{SD}\left[T^{div}\right]$, which represents the standard deviation in the time to divide for cells that have divided at least once. For this parameter, there does not appear to be a significant difference in the estimated value when comparing the two cell types from a single donor, or when comparing two donors and a single cell type. Considering the widths of the relevant box plots, we see that there is larger variation in the parameter estimates obtained for CD8+ T cells than those obtained for CD4+ T cells. In fact, the variation in parameter estimates observed for Donor 1 CD8+ T cells is so large as to suggest that this parameter is not identifiable.

Box plots summarizing estimates for the parameter $\mathrm{E}\left[T^{die}\right]$, which represents the mean time to die for cells that have divided at least once, are shown in Figure 16 of [3]. As was the case with the parameter $\mathrm{SD}\left[T^{div}\right]$, there does not appear to be a significant difference in the estimated value of the parameter $\mathrm{E}\left[T^{die}\right]$ when comparing the two cell types from a single donor, or when comparing two donors and a single cell type. For this parameter, we see that there is larger variation in the parameter estimates obtained for Donor 1 cells (of both types) than those obtained for Donor 2 cells. In fact, the variation in parameter estimates observed for Donor 1 cells is so large that it suggests that this parameter is not identifiable.

In Figure 17 of [3], we provide box plots summarizing estimates for the parameter $\mathrm{SD}\left[T^{die}\right]$, which represents the standard deviation in the time to die for cells that have divided at least once. Similar to the situation observed for $\mathrm{E}\left[T^{die}\right]$, for this parameter there does not appear to be a significant difference in the estimated value when comparing the two cell types from a single donor, or when comparing two donors and a single cell type. Also similar to the situation observed for $\mathrm{E}\left[T^{die}\right]$, we see that there is larger variation in

the estimates for SD $\left[T^{die}\right]$ obtained for Donor 1 cells (of both types) than those obtained for Donor 2 cells. The variation in parameter estimates observed for Donor 1 cells is once again so large that it suggests that the parameter SD $\left[T^{die}\right]$ is also not identifiable.

Box plots summarizing estimates for the parameter F_0, which represents the progressor fraction for undivided cells, are shown in Figure 18 of [3]. It appears that the value of this parameter is larger for CD8+ T cells than for CD4+ T cells in the case of Donor 1 and larger for CD4+ T cells than for CD8+ T cells in the case of Donor 2. When we compare CD4+ T cells obtained from the two distinct donors, there does not appear to be a significant difference in the parameter F_0; however, when comparing CD8+ T cells from the two donors, it appears that F_0 is larger for Donor 1 than for Donor 2.

In Figure 19 of [3], we provide box plots summarizing estimates for the parameter D_μ. There does not appear to be a significant difference in the value of this parameter for CD4+ and CD8+ T cells in the case of Donor 1, but the parameter value is larger for CD8+ T cells in the case of Donor 2. When we compare CD4+ T cells obtained from the two distinct donors, there does not appear to be a significant difference in the parameter D_μ; however, when comparing CD8+ T cells from the two donors, it appears that D_μ is larger for Donor 2 than for Donor 1.

Box plots summarizing estimates for the parameter D_σ are shown in Figure 20 of [3]. It appears that the parameter value is larger for CD8+ T cells than CD4+ T cells in the case of Donor 1, but there does not appear to be a significant difference in the parameter value for CD4+ and CD8+ T cells in the case of Donor 2. When we compare CD4+ T cells obtained from the two distinct donors, it appears that D_σ is larger for Donor 2 than for Donor 1. On the other hand, when comparing CD8+ T cells from the two donors, there does not appear to be a significant difference in the parameter D_σ.

We have already noted that many of our model parameters can be estimated with relatively high reliability, while others do not appear to be identifiable, but thus far all of our arguments have been based upon visual inspection of the box plots in Figures 9 through 20 of [3]. To allow for more careful quantitative analysis of the identifiability of parameters, we provide in Tables 7 through 18 some of the summary statistics used to generate the box plots in those figures. For example, in Table 7 we provide a median and an interquartile range (IQR) corresponding to each of the box plots in Figure 9 of [3]. Since the median and IQR indicate the "center" and "spread", respectively, for a set of parameter estimates, the ratio of these two quantities provides a useful measure of "relative spread". We therefore also include a column for the ratio of IQR to median in each of Tables 7 through 18. When the spread is greater than 50% of the central value for a particular set of parameter estimates (i.e., whenever the ratio of IQR to median is greater than 0.50), we consider the variability in that set of parameter estimates to be "relatively high" and conclude that the parameter may not be identifiable; therefore, the ratios meeting this criteria are emphasized in boldface in the tables. Note that the value 0.50 was chosen somewhat arbitrarily, but comparing Tables 7 through 18 with Figures 9 through 20 of [3] makes it clear that such a value for the ratio of IQR to median does, indeed, indicate a "large" relative spread in a set of parameter estimates.

Based on Tables 7 through 18, we conclude that the model parameters $\mathrm{E}\left[X_a\right]$, $\mathrm{SD}\left[X_a\right]$, c, $\mathrm{E}\left[T_0^{div}\right]$, $\mathrm{SD}\left[T_0^{div}\right]$, $\mathrm{E}\left[T^{div}\right]$, F_0, D_μ, and D_σ can all be estimated with fairly high reliability. On the other hand, the parameters $\mathrm{SD}\left[T^{div}\right]$, $\mathrm{E}\left[T^{die}\right]$, and $\mathrm{SD}\left[T^{die}\right]$ each have very high ratios of IQR to median in some cases, indicating that they may not be identifiable. We conjecture that this could be because the mathematical model is not sensitive to these particular parameters. One might reason, for example, that the lack of model sensitivity to the parameters involving "time until death" occurs because divided cells (those cells for which $i \geq 1$) tend to divide much more often than they die (when considering stimulated T cells from healthy donors) and such behavior can be correctly incorporated into the model as long as the expected time until division, $\mathrm{E}\left[T^{div}\right]$, is significantly smaller than the expected time until death, $\mathrm{E}\left[T^{die}\right]$. To be more specific (and to reuse some terminology that was utilized in Section 5.1), as long as the distribution of the random variable T^{die} tends to be *stochastically larger* (by a substantial margin) than that of T^{div}, the correct dynamical behavior of the system can probably be modeled adequately (at least over the first few days) *even if the parameters describing the distribution of* T^{die} *are not estimated very accurately.* To illustrate this point, consider Figures 10 and 11, in which we plot the (lognormal) distributions of the random variables T^{div} and T^{die} in two different cases. In both cases we use the same set of parameter values for T^{div}, but in each case a different set of a parameter values is used for T^{die}. The values of T^{die} tend to be

larger than those of T^{div} in both cases, so in both situations cells should tend to divide more frequently than they die. (Recall that the fate of any particular cell is determined by whichever of these two random variables produces a *smaller* realization.) We argue that, when all other parameters are fixed using some common set of values, the model output does not vary significantly (at least over the first few days) when the two different sets of parameter values for T^{die} indicated in Figures 10 and 11 are used. To demonstrate this claim, we show sample model output generated using these two different sets of parameter values for T^{die} in Figure 12. The complete sets of parameter values for "Model A" and "Model B" are provided in Table 19. Note that, despite the large discrepancy in the values used for $\mathrm{E}\left[T^{die}\right]$ and $\mathrm{SD}\left[T^{die}\right]$, the output for the two models is indistinguishable until at least Day 4. This simple exercise indicates that the accuracy of data collected in the later days of the experiment may be critical to the correct identification of the parameters $\mathrm{E}\left[T^{die}\right]$ and $\mathrm{SD}\left[T^{die}\right]$.

5.2.2 Parameter Estimates Obtained Using Fixed Values for Some Parameters

By examining scatter plots of various pairings of parameter estimates, we can determine whether or not any correlations might exist between some of the parameters. For example, Figures 13 and 14 indicate a strong

Donor	ViViD Used	Cell Type	Median	IQR	IQR/Median
1	Y	CD4	402.30	32.58	0.0810
1	Y	CD8	680.44	79.29	0.1165
1	N	CD4	388.45	25.33	0.0652
1	N	CD8	678.97	81.78	0.1204
2	Y	CD4	623.98	50.55	0.0810
2	Y	CD8	542.52	21.49	0.0396
2	N	CD4	630.26	82.19	0.1304
2	N	CD8	536.94	24.43	0.0455

Table 7: Summary statistics for estimates of parameter $\mathrm{E}\left[X_a\right]$ (cf. Figure 9 of [3]).

Donor	ViViD Used	Cell Type	Median	IQR	IQR/Median
1	Y	CD4	227.87	17.03	0.0747
1	Y	CD8	339.49	78.22	0.2304
1	N	CD4	215.83	25.02	0.1159
1	N	CD8	335.50	78.12	0.2328
2	Y	CD4	293.16	22.61	0.0771
2	Y	CD8	252.75	15.51	0.0614
2	N	CD4	294.12	39.91	0.1357
2	N	CD8	253.24	16.62	0.0656

Table 8: Summary statistics for estimates of parameter $\mathrm{SD}\left[X_a\right]$ (cf. Figure 10 of [3]).

Donor	ViViD Used	Cell Type	Median	IQR	IQR/Median
1	Y	CD4	0.0069	0.0003	0.0461
1	Y	CD8	0.0077	0.0004	0.0520
1	N	CD4	0.0067	0.0003	0.0487
1	N	CD8	0.0073	0.0004	0.0609
2	Y	CD4	0.0068	0.0003	0.0448
2	Y	CD8	0.0039	0.0006	0.1424
2	N	CD4	0.0065	0.0002	0.0343
2	N	CD8	0.0040	0.0004	0.0932

Table 9: Summary statistics for estimates of parameter c (cf. Figure 11 of [3]).

Donor	ViViD Used	Cell Type	Median	IQR	IQR/Median
1	Y	CD4	63.02	2.28	0.0362
1	Y	CD8	50.20	2.34	0.0466
1	N	CD4	62.10	1.92	0.0308
1	N	CD8	49.68	3.61	0.0726
2	Y	CD4	60.26	1.36	0.0226
2	Y	CD8	48.49	1.06	0.0218
2	N	CD4	63.42	2.23	0.0351
2	N	CD8	47.54	1.07	0.0226

Table 10: Summary statistics for estimates of parameter E $\left[T_0^{div}\right]$ (cf. Figure 12 of [3]).

Donor	ViViD Used	Cell Type	Median	IQR	IQR/Median
1	Y	CD4	28.07	1.63	0.0580
1	Y	CD8	19.21	1.92	0.0998
1	N	CD4	27.20	1.79	0.0658
1	N	CD8	18.08	4.30	0.2377
2	Y	CD4	23.90	1.00	0.0418
2	Y	CD8	18.56	0.89	0.0478
2	N	CD4	26.62	1.91	0.0719
2	N	CD8	17.49	0.81	0.0464

Table 11: Summary statistics for estimates of parameter SD $\left[T_0^{div}\right]$ (cf. Figure 13 of [3]).

Donor	ViViD Used	Cell Type	Median	IQR	IQR/Median
1	Y	CD4	10.96	0.74	0.0672
1	Y	CD8	10.39	1.33	0.1276
1	N	CD4	11.21	0.70	0.0623
1	N	CD8	10.89	1.79	0.1640
2	Y	CD4	8.96	0.81	0.0908
2	Y	CD8	8.97	0.51	0.0569
2	N	CD4	8.97	0.75	0.0833
2	N	CD8	9.20	0.46	0.0505

Table 12: Summary statistics for estimates of parameter E $\left[T^{div}\right]$ (cf. Figure 14 of [3]).

Donor	ViViD Used	Cell Type	Median	IQR	IQR/Median
1	Y	CD4	0.86	0.73	**0.8428**
1	Y	CD8	1.47	4.09	**2.7912**
1	N	CD4	0.89	0.12	0.1342
1	N	CD8	4.25	5.67	**1.3347**
2	Y	CD4	0.80	0.08	0.0988
2	Y	CD8	0.94	0.44	0.4648
2	N	CD4	0.82	0.04	0.0507
2	N	CD8	1.00	0.61	**0.6087**

Table 13: Summary statistics for estimates of parameter SD $\left[T^{div}\right]$ (cf. Figure 15 of [3]).

Donor	ViViD Used	Cell Type	Median	IQR	IQR/Median
1	Y	CD4	38.49	43.14	**1.1207**
1	Y	CD8	71.96	66.02	**0.9175**
1	N	CD4	37.90	32.78	**0.8650**
1	N	CD8	71.68	76.91	**1.0729**
2	Y	CD4	40.84	5.82	0.1426
2	Y	CD8	50.67	24.57	0.4848
2	N	CD4	37.83	16.64	0.4397
2	N	CD8	49.75	20.40	0.4100

Table 14: Summary statistics for estimates of parameter E $\left[T^{die}\right]$ (cf. Figure 16 of [3]).

Donor	ViViD Used	Cell Type	Median	IQR	IQR/Median
1	Y	CD4	1.85	64.21	**34.7682**
1	Y	CD8	27.30	66.82	**2.4481**
1	N	CD4	1.79	64.90	**36.1615**
1	N	CD8	45.91	59.70	**1.3004**
2	Y	CD4	20.56	5.54	0.2693
2	Y	CD8	39.72	25.11	**0.6322**
2	N	CD4	39.68	23.65	**0.5960**
2	N	CD8	41.82	25.57	**0.6113**

Table 15: Summary statistics for estimates of parameter SD $\left[T^{die}\right]$ (cf. Figure 17 of [3]).

Donor	ViViD Used	Cell Type	Median	IQR	IQR/Median
1	Y	CD4	0.7092	0.0388	0.0547
1	Y	CD8	0.8588	0.0350	0.0408
1	N	CD4	0.6812	0.0421	0.0619
1	N	CD8	0.8840	0.0434	0.0491
2	Y	CD4	0.6429	0.0248	0.0386
2	Y	CD8	0.5293	0.0496	0.0937
2	N	CD4	0.6574	0.0392	0.0597
2	N	CD8	0.4613	0.0453	0.0982

Table 16: Summary statistics for estimates of parameter F_0 (cf. Figure 18 of [3]).

Donor	ViViD Used	Cell Type	Median	IQR	IQR/Median
1	Y	CD4	3.75	0.68	0.1801
1	Y	CD8	3.91	1.19	0.3034
1	N	CD4	3.75	0.34	0.0913
1	N	CD8	3.42	1.00	0.2913
2	Y	CD4	3.82	0.36	0.0939
2	Y	CD8	4.92	0.43	0.0874
2	N	CD4	3.76	0.89	0.2373
2	N	CD8	5.01	0.40	0.0803

Table 17: Summary statistics for estimates of parameter D_μ (cf. Figure 19 of [3]).

Donor	ViViD Used	Cell Type	Median	IQR	IQR/Median
1	Y	CD4	1.10	0.24	0.2172
1	Y	CD8	1.83	0.66	0.3583
1	N	CD4	1.08	0.15	0.1398
1	N	CD8	1.98	0.57	0.2877
2	Y	CD4	1.76	0.41	0.2349
2	Y	CD8	1.66	0.33	0.1968
2	N	CD4	1.76	0.49	0.2813
2	N	CD8	1.61	0.35	0.2169

Table 18: Summary statistics for estimates of parameter D_σ (cf. Figure 20 of [3]).

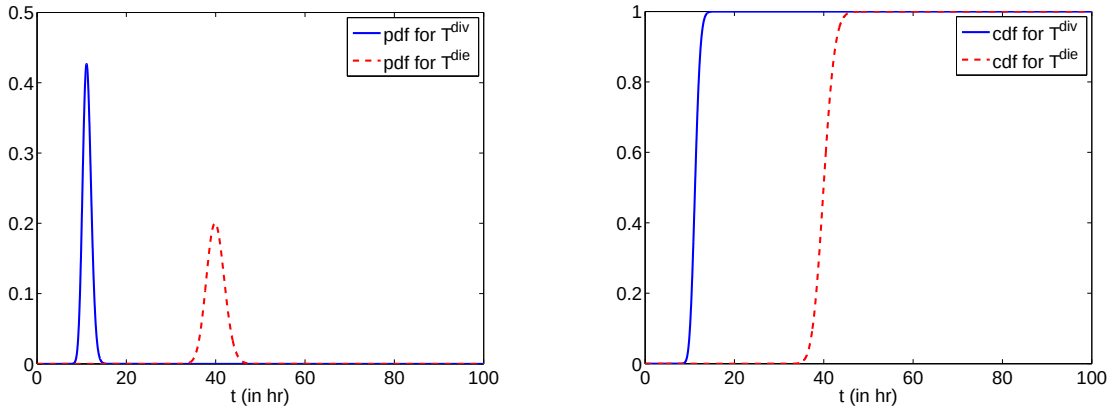

(a) (b)

Figure 10: Plots illustrating the (a) pdfs and (b) cdfs of the lognormally distributed random variables T^{div} and T^{die} when $\mathrm{E}\left[T^{div}\right] = 11.21$, $\mathrm{SD}\left[T^{div}\right] = 0.89$, $\mathrm{E}\left[T^{die}\right] = 40$, and $\mathrm{SD}\left[T^{die}\right] = 2$.

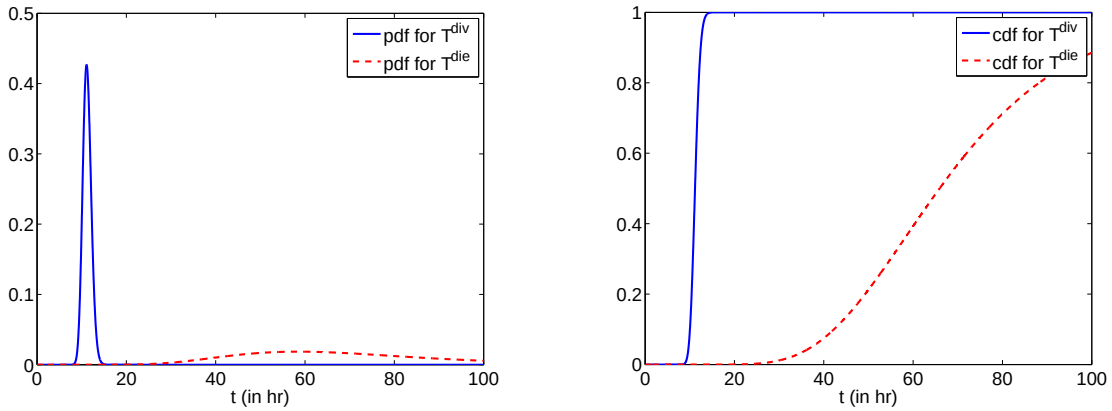

(a) (b)

Figure 11: Plots illustrating the (a) pdfs and (b) cdfs of the lognormally distributed random variables T^{div} and T^{die} when $\mathrm{E}\left[T^{div}\right] = 11.21$, $\mathrm{SD}\left[T^{div}\right] = 0.89$, $\mathrm{E}\left[T^{die}\right] = 70$, and $\mathrm{SD}\left[T^{die}\right] = 25$.

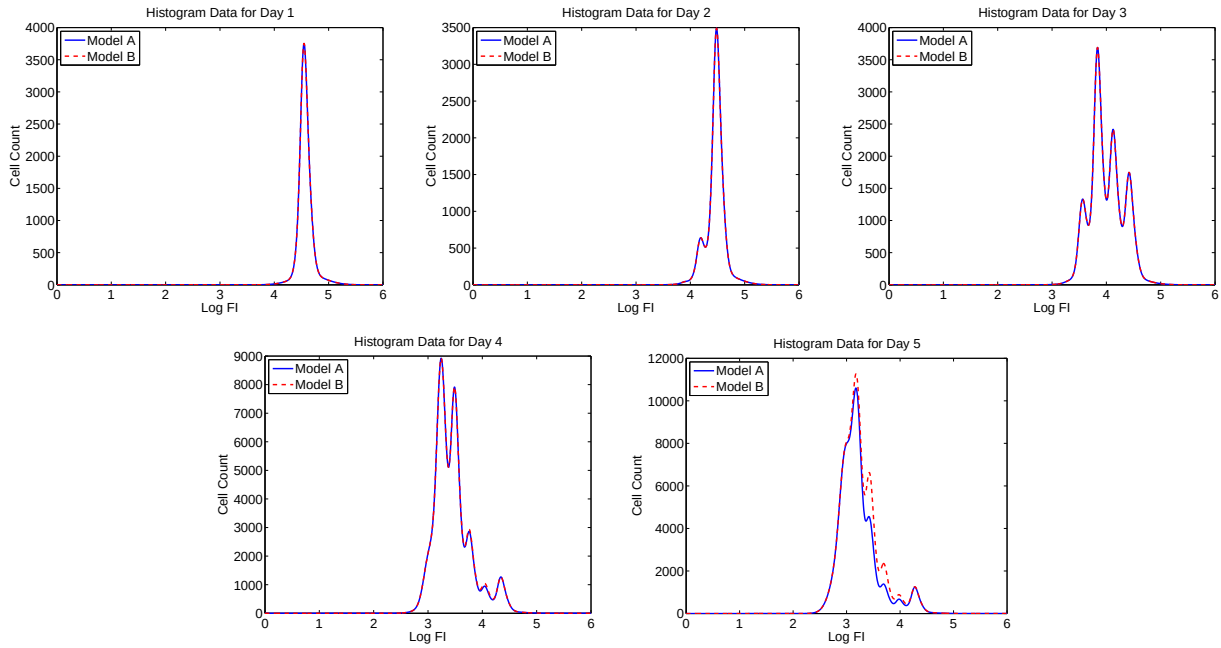

Figure 12: Summary histogram output for Model A, in which $\mathrm{E}\left[T^{die}\right] = 40$ and $\mathrm{SD}\left[T^{die}\right] = 2$, and Model B, in which $\mathrm{E}\left[T^{die}\right] = 70$ and $\mathrm{SD}\left[T^{die}\right] = 25$. The time points corresponding to "Day 1" through "Day 5" are the same as those that were used for data collection as described in Section 2.

Parameter	Model A	Model B
$\mathrm{E}\left[X_a\right]$	388.45	388.45
$\mathrm{SD}\left[X_a\right]$	215.83	215.83
c	0.0067	0.0067
$\mathrm{E}\left[T_0^{div}\right]$	62.10	62.10
$\mathrm{SD}\left[T_0^{div}\right]$	27.20	27.20
$\mathrm{E}\left[T^{div}\right]$	11.21	11.21
$\mathrm{SD}\left[T^{div}\right]$	0.89	0.89
$\mathrm{E}\left[T^{die}\right]$	**40.00**	**70.00**
$\mathrm{SD}\left[T^{die}\right]$	**2.00**	**25.00**
F_0	0.6812	0.6812
D_μ	3.75	3.75
D_σ	1.08	1.08

Table 19: Parameter values used to obtain summary histogram output for Models A and B in Figure 12. Values which differ in the two models are emphasized in boldface.

correlation between the parameters $\mathrm{E}\left[T_0^{div}\right]$ and $\mathrm{SD}\left[T_0^{div}\right]$ and $\mathrm{E}\left[T^{die}\right]$ and $\mathrm{SD}\left[T^{die}\right]$, respectively. We therefore implemented a variation of our parameter estimation scheme in which one or more of the 12 model parameters can be fixed, hoping that this might reduce the variability seen in some of the other parameter estimates.

Based on the relationships suggested by Figures 13 and 14, we applied our modified parameter estimation algorithm in three scenarios: (i) using fixed values for $\mathrm{E}\left[T_0^{div}\right]$, (ii) using fixed values for $\mathrm{E}\left[T^{die}\right]$, and (iii) using fixed values for both $\mathrm{E}\left[T_0^{div}\right]$ and $\mathrm{E}\left[T^{die}\right]$. We chose to fix the values of the two selected parameters at the (approximate) median estimates obtained from the basic parameter estimation scheme (with no fixed parameters). Since these medians vary for the different combinations of donor, ViViD dye status, and cell type, we used different fixed values for each of these combinations. The specific fixed values used for $\mathrm{E}\left[T_0^{div}\right]$ and $\mathrm{E}\left[T^{die}\right]$ are shown in Tables 20 and 21, respectively. Our goal in fixing the value of one or more parameters is to reduce the variability in the parameter estimates for other parameters, so we need to select some measure of variability for the analysis. Throughout the discussions that follow, we will use the interquartile range (IQR) as a rough measure of variability in the parameter estimates for a given combination of donor, ViViD dye status, and cell type.

The results of applying our modified parameter estimation technique in case (i) are shown in Figures 23 through 33 of [3]. Note that the total number of figures is 11 – there is one for each model parameter except $\mathrm{E}\left[T_0^{div}\right]$, which is fixed. Comparing Figures 23 through 33 of [3] with Figures 9 through 20 of [3] (or, more precisely, comparing the IQRs for the corresponding box plots in those figures) reveals that fixing the value of $\mathrm{E}\left[T_0^{div}\right]$ is *not* a universally advantageous approach if our goal is to reduce variability in the parameter estimates. Interestingly, this approach is almost always advantageous in the case of Donor 1 data, but for many of the parameter estimates this approach causes an *increase* in variability when considering the Donor 2 data. For example, estimates for $\mathrm{E}\left[X_a\right]$, $\mathrm{SD}\left[X_a\right]$, $\mathrm{SD}\left[T_0^{div}\right]$, $\mathrm{E}\left[T^{die}\right]$, $\mathrm{SD}\left[T^{die}\right]$, and D_μ all experience significant increases in variability for at least some of the combinations of ViViD dye status and cell type when considering Donor 2 data.

In Figures 34 through 44 of [3], we show the results of applying our modified parameter estimation

Donor	ViViD Used	Cell Type	$\mathrm{E}\left[T_0^{div}\right]$
1	Y	CD4	64
1	Y	CD8	51
1	N	CD4	62.5
1	N	CD8	49
2	Y	CD4	60.5
2	Y	CD8	48
2	N	CD4	64
2	N	CD8	47

Table 20: Parameter values used when fixing the parameter $\mathrm{E}\left[T_0^{div}\right]$.

Donor	ViViD Used	Cell Type	$\mathrm{E}\left[T^{die}\right]$
1	Y	CD4	40
1	Y	CD8	62
1	N	CD4	40
1	N	CD8	62
2	Y	CD4	40
2	Y	CD8	52
2	N	CD4	36
2	N	CD8	50

Table 21: Parameter values used when fixing the parameter $\mathrm{E}\left[T^{die}\right]$.

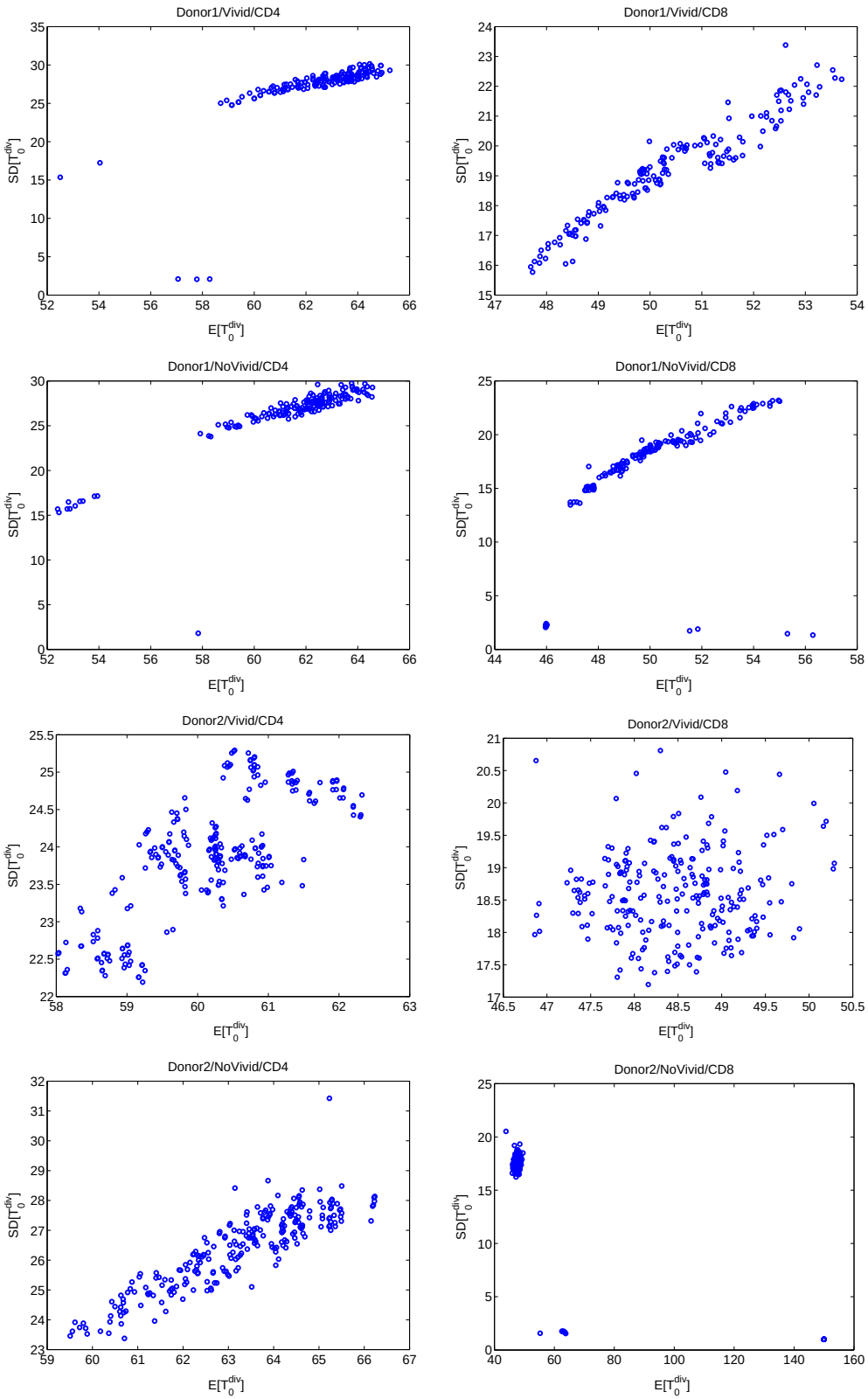

Figure 13: Scatterplots illustrating a correlation between E $\left[T_0^{div}\right]$ and SD $\left[T_0^{div}\right]$.

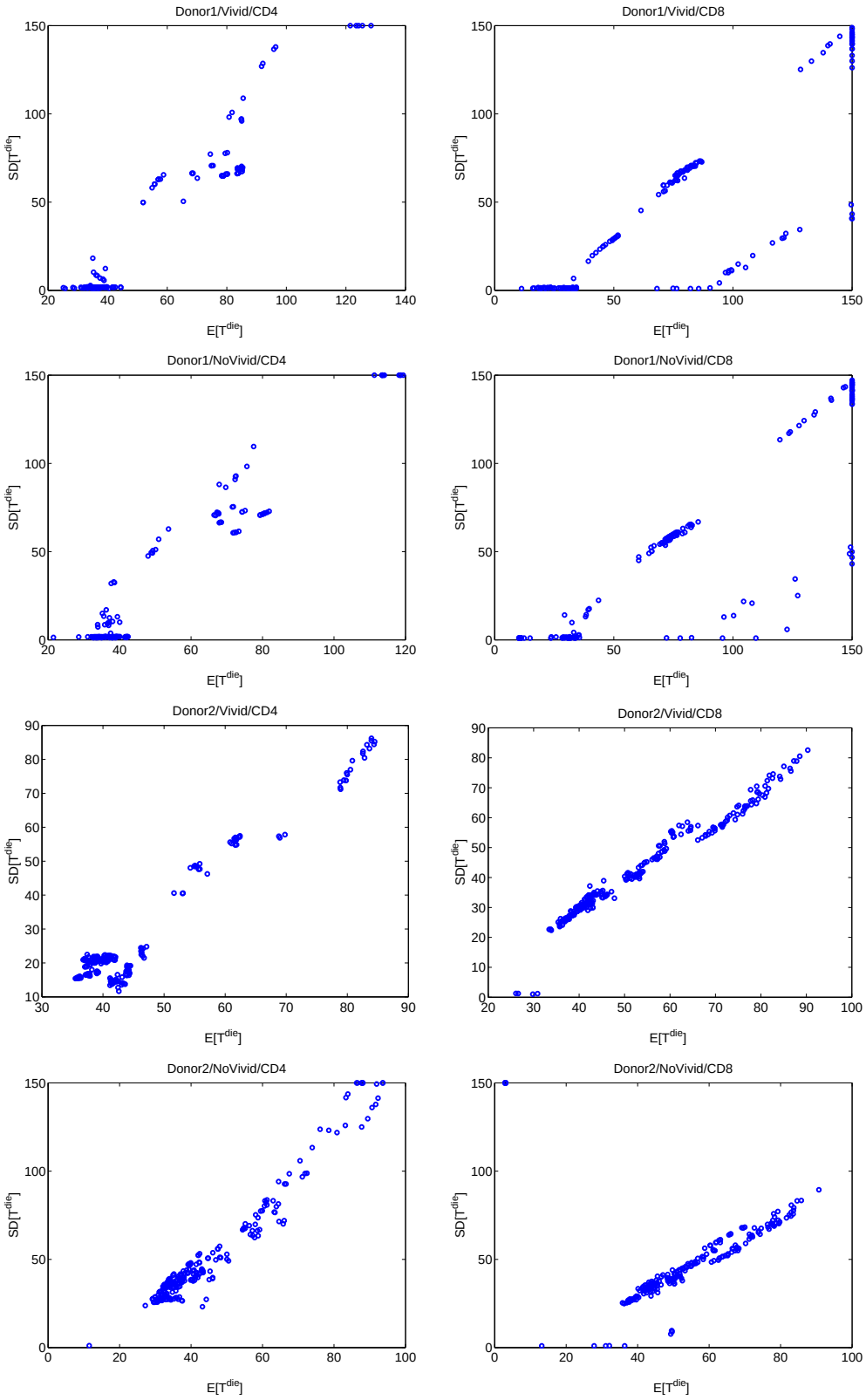

Figure 14: Scatterplots illustrating a correlation between E $\left[T^{die}\right]$ and SD $\left[T^{die}\right]$.

technique in case (ii). Again, note that there is one figure for each of the 11 model parameters that is not fixed. Comparing Figures 34 through 44 of [3] with Figures 9 through 20 of [3], it is evident that fixing the value of $\mathrm{E}\left[T^{die}\right]$ causes increases in the variability of parameter estimates in many cases. Unlike the situation with the previous fixed parameter ($\mathrm{E}\left[T_0^{div}\right]$), these increases are prevalent when considering Donor 1 data *and* Donor 2 data. We are therefore forced to conclude that fixing the value of $\mathrm{E}\left[T^{die}\right]$ also fails as a universally advantageous scheme for reducing variability in the parameter estimates.

Finally, the results of applying our modified parameter estimation technique in case (iii) are shown in Figures 45 through 54 of [3]. This time, there are a total 10 model parameters that are not fixed, and hence there are 10 figures in this list. Following the same analytical approach described for the previous parameter-fixing cases, we conclude that simultaneously fixing the values of $\mathrm{E}\left[T_0^{div}\right]$ and $\mathrm{E}\left[T^{die}\right]$ fails as a universally advantageous scheme for reducing variability in the parameter estimates.

5.2.3 Parameter Estimates Obtained Using Only Data for Days 1 through 3

As was demonstrated in Section 5.1, the amount of relative variation in the cell counts undergoes significant changes between Day 3 and Day 5. We therefore also attempted to estimate parameters using only data from Days 1 through 3. The results of applying our parameter estimation technique to such reduced data sets are provided in Figures 55 through 66 of [3]. Since in this case we have triplicate samples for each of *three* days, there are $3^3 = 27$ possible ways to form a three-day time series data set for each donor. Therefore, each box plot in the above-referenced figures represents a summary of 27 parameter estimates.

Comparing Figures 55 through 66 of [3] with Figures 9 through 20 of [3] reveals that there are clear differences between the parameter estimates obtained using three-day data sets and those obtained using complete data sets. For a complete discussion of the differences, see Section 5.2.5 of [3]. This outcome further supports the evidence given in Section 5.1 that the periodic exchange of nutrient medium starting at Day 3 causes changes to the counts and/or the proliferative behavior (as described by our cyton-based dynamical models) of the affected cell cultures.

6 Conclusion

In this document, we have presented the findings of our recent investigation into the variability that exists in CFSE-based flow cytometry data in the context of cyton-based mathematical models for cell proliferation. We have described the specific mathematical model that we consider, as well as a weighted least squares scheme that allows one to estimate the parameters in that mathematical model using CFSE flow cytometry data. By applying our parameter estimation scheme to a large body of data, we were able to assess both experimental and biological variability in the resulting parameter estimates. In this section of the document, we will summarize our findings and utilize them to make some important conclusions concerning both standard CFSE flow cytometry experimental procedures and the current generation of mathematical models that are used to analyze data that result from these procedures.

We begin by summarizing our results concerning identifiability of the various parameters in our model. As was discussed in Section 5.2.1, it appears that the parameters $\mathrm{E}\left[X_a\right]$, $\mathrm{SD}\left[X_a\right]$, c, $\mathrm{E}\left[T_0^{div}\right]$, $\mathrm{SD}\left[T_0^{div}\right]$, $\mathrm{E}\left[T^{div}\right]$, F_0, D_μ, and D_σ can all be estimated with fairly high reliability, while the parameters $\mathrm{SD}\left[T^{div}\right]$, $\mathrm{E}\left[T^{die}\right]$, and $\mathrm{SD}\left[T^{die}\right]$ do not appear to be identifiable. As a possible explanation of this, we proposed that the model may not be sensitive to the parameters involving T^{die} at the earlier time points (i.e., Days 1 through 3). We also provided an example (cf. Figures 10 through 12) which indicated that the model may be more sensitive to these parameters at the later time points (i.e., by Day 5). Unfortunately, another key finding of this study is that the accuracy of *in vitro* CFSE flow cytometry data appears to decrease significantly after Day 3. We hypothesize that cell culturing protocols (and specifically the depletion and replenishment of nutrient medium) lead to increase of variability in measured triplicate data after Day 3.

A number of differences between the parameter estimates observed for distinct donors and cell types are outlined in Section 5.2.1, but it is difficult to state the relationships described there in a more concise way. We would like to revisit, however, one interesting general result that arose in Section 5.2.1: the use of ViViD dye does not seem to have a significant effect on the estimates obtained for most of the model

parameters. Interestingly, the largest fractions of dead cells are typically identified (using ViViD) in the first three days of the experiment (cf. Tables 2 through 6); i.e., the largest relative errors in cell counts due to the counting of dead cells (when not using ViViD to omit them) occurs in the earliest days of the experiment. This may be because the large die-off of cells that occurs immediately following PHA stimulation (which was mentioned in Section 3.5) leaves a considerable number of dead (but not yet disintegrated) cells in its wake at the beginning of the experiment. Presumably these cells are able to disintegrate completely by Day 4, at which point the fractions of dead cells identified using ViViD are much smaller. Whatever the reason, it seems that errors in cell counts caused by the inclusion of dead cells are likely to be largest when errors in the true cell counts, themselves, are smallest (cf. Section 5.1). Also, errors in cell counts caused by the inclusion of these cells are likely to be smallest when errors in the true cell counts, themselves, are largest. So, although the use of ViViD dye may not appear to be beneficial in the estimation of parameters based on the results of this study, use of ViViD may prove to be beneficial in later studies if new techniques make it possible to obtain more precise true cell counts.

We implemented several variations to our basic parameter estimation scheme in an attempt to reduce variability in parameter estimates. In Section 5.2.2, we discussed the results of fixing the values of $\mathrm{E}\left[T_0^{div}\right]$, $\mathrm{E}\left[T^{die}\right]$, or both $\mathrm{E}\left[T_0^{div}\right]$ and $\mathrm{E}\left[T^{die}\right]$, and concluded that none of these schemes proved to be universally beneficial. In fact, in many cases these approaches tended to *increase* variability in parameter estimates.

We also implemented a variation of our basic parameter estimation scheme in which only data from Days 1 through 3 were utilized. As was outlined in Section 5.2.3, clear differences exist between the parameter estimates obtained using three-day data sets and those obtained using complete data sets. This outcome, along with the evidence presented in Section 5.1, seems to indicate that the periodic exchange of nutrient medium starting at Day 3 does affect the proliferation of cells in the cell culture wells that are processed after Day 3. Furthermore, the very fact that the exchange of nutrient medium is necessary allows one to infer that cell cultures deplete nutrients in their respective wells throughout the experiment. Such changes in the cell culture environments unfortunately contradict the underlying assumptions of our model. In particular, the cyton model that we've incorporated into our mass- and energy-conserving mathematical model tacitly assumes a *constant environment* for cultures of proliferating cells. (Note that the time-dependence of the cytons $\{(\phi_i(t), \psi_i(t))\}$ is actually based on "time since the last division occurred", or time in the frame of reference of an individual cell. The cytons therefore have no dependence on "real time", or time in the frame of reference of the experimenter. In real time, the conditions in the nutrient medium are apparently changing, and the basic cyton model is not capable of handling such a non-constant environment.) Thus, several observations made in this report indicate that *the standard cell culturing protocol used for CFSE flow cytometry experiments does not provide a constant environment for cells growing in the wells.* Adjustments could be made to the model, of course, to allow for time-dependence of the cytons, but any such adjustments would most likely lead to overparameterization; i.e., the increase in the number of parameters required by such adjustments would probably lead to even further identifiability issues. Furthermore, environmental changes caused by the exchange of the nutrient medium at discrete time points would probably be very difficult to quantify. It is worth noting that, in cases where a smaller total number of cells is stimulated (e.g., in response to antigen-specific challenges) the depletion of nutrient medium may not be significant over the course of a five-day experiment; thus, the exchange of nutrient medium may be unnecessary in such cases.

As a final point, we would like to re-emphasize that typical CFSE flow cytometry data *are not truly longitudinal* (cf. Section 2). For this reason, it appears that our ability to validate (and estimate parameters for) the latest generation of division- and label-structured cell population models (presented here) is limited by the precision with which experimenters can seed a set of cell culture wells. (Recall that, upon seeding, we assume all wells to be identical in that they include the same numbers of total cells in the same proportions.) The results presented in this report suggest that the use of time series data which are not truly longitudinal (which is the current standard protocol for *in vitro* CFSE flow cytometry experiments) leads to high variability in estimates for many of the relevant parameters in our model. This could be because the numbers of cells used to seed two distinct wells, which are assumed to be identical and which will be harvested and analyzed to produce data for two distinct points in the time series, can differ by 16 percent or more (cf. Table 2). (We should mention here the possibility that experimenters may actually seed the wells with much higher precision than seems to be the case, and that poor precision in *bead counts* might be the

true cause of the apparent discrepancies in total cell numbers. This possibility was considered in [2], and a statistical model was formulated there to account for errors in bead counts, but we believe such a model adjustment leads to overparameterization.) This issue of poor precision in total cell counts, along with the issue of non-constant environment, suggests that substantive changes to CFSE flow cytometry and *in vitro* cell culturing protocol and/or significant modifications to our mathematical model need to be considered.

We reiterate that, for this study, we have only considered PHA-stimulated cells. Because it is a *non-specific* T cell mitogen, PHA stimulates *all* T cells to begin dividing and therefore leads to a somewhat artificial situation from an immunological perspective. Nevertheless, the methods and results presented in this report indicate that many of the important and biologically relevant parameters for describing T cell proliferation can be reliably estimated using our approach. As more realistic and interesting experiments are devised and carried out (e.g., Gag protein stimulation of cells from HIV-positive donors), it is our hope that the challenges and concerns presented here will be utilized to develop and select models that account for variability in experimental data.

Acknowledgments

This research was supported in part by Grant Number NIAID R01AI071915-10 from the National Institute of Allergy and Infectious Diseases, in part by the National Science Foundation under Research Training Grant (RTG) DMS-0636590, and in part by grant SAF2010-21336 from the Spanish Ministry of Science and Innovation. The authors are also grateful to Brian Reich, who made himself available for consultations regarding statistical hypothesis testing and provided several useful suggestions during the preparation of this manuscript.

References

[1] H.T. Banks, A. Choi, T. Huffman, J. Nardini, L. Poag, W.C. Thompson, Quantifying CFSE label decay in flow cytometry data, CRSC-TR12-20, North Carolina State University, December 2012; *Applied Math. Letters* **26** (2013), 571–577.

[2] H.T. Banks, D.F. Kapraun, W. Clayton Thompson, Cristina Peligero, Jordi Argilaguet, and Andreas Meyerhans, A novel statistical analysis and interpretation of flow cytometry data, CRSC-TR12-23, North Carolina State University, March 2013; *J. Biological Dynamics*, **7** (2013), 96–132.

[3] H.T. Banks, D.F. Kapraun, Kathryn G. Link, W. Clayton Thompson, Cristina Peligero, Jordi Argilaguet, and Andreas Meyerhans, Experimental and biological variability in CFSE-based flow cytometry data, CRSC-TR13-10, North Carolina State University, September 2013.

[4] H.T. Banks, Zackary R. Kenz, and W. Clayton Thompson, An Extension of RSS-based Model Comparison Tests for Weighted Least Squares, CRSC-TR12-18, North Carolina State University, August 2012; *Intl. J. Pure and Appl. Math.* **79** (2012).

[5] H.T. Banks, Karyn L. Sutton, W. Clayton Thompson, G. Bocharov, Marie Doumic, Tim Schenkel, Jordi Argilaguet, Sandra Giest, Cristina Peligero, and Andreas Meyerhans, A new model for the estimation of cell proliferation dynamics using CFSE data, CRSC-TR11-05, North Carolina State University, Revised July 2011; *J. Immunological Methods,* **373** (2011), 143–160; DOI:10.1016/j.jim.2011.08.014.

[6] H.T. Banks and W. Clayton Thompson, A division-dependent compartmental model with cyton and intracellular label dynamics, CRSC-TR12-12, North Carolina State University, May 2012; *Intl. J. Pure and Appl. Math* **77** (2012), 119–147.

[7] H.T. Banks and W. Clayton Thompson, Mathematical models of dividing cell populations: Application to CFSE data, CRSC-TR12-10, North Carolina State University, April 2012; *J. Math. Modeling of Natural Phenomena* **7** (2012), 24–52.

[8] H.T. Banks and H.T. Tran, *Mathematical and Experimental Modeling of Physical and Biological Processes*, CRC Press, Boca Raton London New York, 2009.

[9] G. Bocharov, T. Luzyanina, J. Cupovic, and B. Ludewig, Asymmetry of cell division in CFSE-based lymphocyte proliferation analysis, *Front. Immunol.* **4**:264 (2013); DOI:10.3389/fimmu.2013.00264.

[10] M. Davidian and D.M. Giltinan, *Nonlinear Models for Repeated Measurement Data*, Chapman and Hall, London, 2000.

[11] J. Hasenauer, D. Schittler, and F. Allgöwer, Analysis and simulation of division- and label-structured population models: a new tool to analyze proliferation assays, *Bull. Math. Biol.* **74** (2012), 2692–2732.

[12] E.D. Hawkins, Mirja Hommel, M.L Turner, Francis Battye, J Markham and P.D Hodgkin, Measuring lymphocyte proliferation, survival and differentiation using CFSE time-series data, *Nature Protocols*, **2** (2007), 2057–2067.

[13] E.D. Hawkins, M.L. Turner, M.R. Dowling, C. van Gend, and P.D. Hodgkin, A model of immune regulation as a consequence of randomized lymphocyte division and death times, *Proc. Natl. Acad. Sci.*, **104** (2007), 5032–5037.

[14] E.L. Lehmann, *Nonparametrics: Statistical Methods Based on Ranks*, Holden-Day, San Francisco, 1975.

[15] A. B. Lyons, J. Hasbold and P.D. Hodgkin, Flow cytometric analysis of cell division history using dilution of carboxyfluorescein diacetate succinimidyl ester, a stably integrated fluorescent probe, *Methods in Cell Biology*, **63** (2001), 375–398.

[16] A.B. Lyons and C.R. Parish, Determination of lymphocyte division by flow cytometry, *J. Immunological Methods*, **171** (1994), 131–137.

[17] B. Quah, H. Warren, and C. Parish, Monitoring lymphocyte proliferation in vitro and in vivo with the intracellular fluorescent dye carboxyfluorescein diacetate succinimidyl ester, *Nature Protocols*, **2** (2007), 2049–2056.

[18] D. Schittler, J. Hasenauer, and F. Allgöwer, A generalized model for cell proliferation: Integrating division numbers and label dynamics, *Proc. Eighth International Workshop on Computational Systems Biology (WCSB 2011)*, June 2011, Zurich, Switzerland, p. 165–168.

[19] G.A. Seber and C.J. Wild, *Nonlinear Regression*, Wiley, Hoboken, NJ, 2003.

[20] W. Clayton Thompson, *Partial Differential Equation Modeling of Flow Cytometry Data from CFSE-based Proliferation Assays,* Ph.D. Dissertation, Dept. of Mathematics, North Carolina State University, Raleigh, December, 2011.

[21] R. Sennerstam, Partition of protein (mass) to sister cell pairs at mitosis: a re-evaluation, *J. Cell. Sci.* **90** (1988), 301–306.

[22] S.A. Weston and C.R. Parish, New fluorescent dyes for lymphocyte migration studies: Analysis by flow cytometry and fluorescence microscopy, *J. Immunological Methods*, **133** (1990), 87-97.